haematologica
Journal of the Ferrata Storti Foundation

TGFβ-activated kinase-1 knockdown in hematopoietic stem-progenitor cells causes PANoptosis and myelodysplastic syndrome-like disease in mice

by Lei Zhang, Wenyan Li, Rohit Thalla, Rongyao Ma, Ryan Mack, Ameet R. Kini, Austin Runde, Patrick A. Hagen, Kevin Barton, Jorgena Kosti-Schwartz, Peter Breslin, Hong-Long Ji and Jiwang Zhang

Received: April 7, 2025.
Accepted: October 20, 2025.

Citation: Lei Zhang, Wenyan Li, Rohit Thalla, Rongyao Ma, Ryan Mack, Ameet R. Kini, Austin Runde, Patrick A. Hagen, Kevin Barton, Jorgena Kosti-Schwartz, Peter Breslin, Hong-Long Ji and Jiwang Zhang. TGFβ-activated kinase-1 knockdown in hematopoietic stem-progenitor cells causes PANoptosis and myelodysplastic syndrome-like disease in mice.
Haematologica. 2025 Oct 30. doi: 10.3324/haematol.2025.287951 [Epub ahead of print]

TGFβ-activated kinase-1 knockdown in hematopoietic stem-progenitor cells causes PANoptosis and myelodysplastic syndrome-like disease in mice

Lei Zhang[1,2,3], Wenyan Li[4], Rohit Thalla[2,3], Rongyao Ma[1], Ryan Mack[2,3], Ameet R. Kini[5], Austin Runde[2,3], Patrick A. Hagen[2,6], Kevin Barton[2,6], Jorgena Kosti-Schwartz[2,5], Peter Breslin[2,3,7], Hong-Long Ji[8], Jiwang Zhang[2,3,5*]

[1] Cyrus Tang Hematology Center, Collaborative Innovation Center of Hematology, National Clinical Research Center for Hematologic Diseases, MOE Engineering Center of Hematological Disease, Soochow University, Suzhou 215123, China

[2] Oncology Institute, Cardinal Bernardin Cancer Canter, Loyola University Chicago Medical Center, Maywood, IL 60153, USA

[3] Department of Cancer Biology, Loyola University Chicago Medical Center, Maywood, IL 60153, USA

[4] Lanzhou University Second Hospital, Key Laboratory of Urological Diseases in Gansu Province, Lanzhou, Gansu 730030, China

[5] Departments of Pathology and Radiation Oncology, Loyola University Chicago Medical Center, Maywood, IL 60153, USA

[6]Department of Medicine, Loyola University Chicago Medical Center, Maywood, IL 60153, USA

[7] Departments of Biology and Molecular/Cellular Physiology, Loyola University Chicago, Maywood, IL 60153, USA

[8] Department of Surgery, Loyola University Chicago Medical Center, Maywood, IL 60153, USA

Authors' contributions: LZ, WL and JWZ designed the experiments, analyzed the data, and drafted the manuscript. JWZ supervised the overall research, designed the experiments, analyzed the data, and edited the manuscript; LZ, WL, RT, RYM, RM, AK, AR, PH, KB, JKS, JK, PB, HLJ, and JWZ collectively contributed to data collection and interpretation of the results. AK, PH, KB and JKS provided study samples, clinical data, and helped to revise the manuscript. PB and JWZ helped to write and also edited and refined the manuscript.

Running heads: *Tak1* knockdown causes MDS-like diseases in mice.

***Corresponding author**: Jiwang Zhang, jzhang@luc.edu

Data-sharing statement: Original data, protocols and reagents are available to other investigators upon request.

Conflict of interest statement: The authors declare no conflict interests.

Acknowledgments: The authors thank the staff of the Department of Comparative Medicine at Loyola University Medical Center for their excellent animal care services, as well as Ms. Patricia Simms for flow cytometric sorting of HSCs and progenitors.

Funding: This work was supported by NIH grants NHLBI R01 HL133560, NCI R01 CA223194 and NCI R01 CA301049 through Loyola University Chicago as well as by Loyola Program Development funding to Jiwang Zhang. It was also supported by Interdisciplinary Basic Frontier Innovation Program of Suzhou Medical College of Soochow University (YXY2304063), and the Priority Academic Program Development of Jiangsu Higher Education Institutions (PAPD).

Abstract

Mutant *SF3B1* (*SF3B1*^{mut}) in hematopoietic stem/progenitor cells (HSPCs) primarily affects erythropoiesis, resulting in myelodysplastic syndromes (MDS) with refractory macrocytic anemia and ring sideroblasts. *SF3B1*^{mut} results in aberrant splicing of a large number of transcripts in HSPCs due to the alternative use of cryptic splice sites. Aberrant splicing of *Tmem14c* and *Abcb7* has been shown to be the cause of the ring sideroblasts. However, the key mis-spliced gene(s) that drive macrocytic anemia have not been well-determined. Mis-splicing and downregulation of *TAK1* pre-mRNA was detected in *SF3B1*^{mut}-HSPCs. We found that TAK1 is required for the survival of HSPCs by restricting RIPK1 dependent and independent PANoptosis. PANoptosis was increased in bone marrow samples from *SF3B1*^{mut}-MDS patients. To study whether TAK1-downregulation is the cause of anemia in *SF3B1*^{mut}-MDS, we knocked down *Tak1* (*Tak1*^{KD}) in mouse HSPCs. We found that mice transplanted with *Tak1*^{KD}-HSPCs developed anemia and that Ripk1 inhibition could restore blood cell counts in such anemic mice. *Tak1*^{KD}-HSPCs are highly sensitive to TAK1 inhibitor- or cIAP inhibitor-induced PANoptosis. Furthermore, RIPK1 inhibition could also correct differentiation and survival defects of *SF3B1*^{mut} human erythroblasts (EBs). TAK1 inhibitor could also preferentially eliminate *SF3B1*^{mut} HSPCs from MDS patient samples. Our study suggests that *SF3B1*^{mut} MDS can be treated by either inhibition of RIPK1-PANoptotic signaling to restore blood cell counts or activation of PANoptosis to eliminate the mutant HSPCs.

Introduction

Myelodysplastic syndromes (MDS) are a heterogeneous group of preleukemic diseases which are characterized by persistent peripheral blood (PB) cytopenia, morphologic dysplasia, and a high risk of transformation to acute myeloid leukemia (AML).[1] The incidence rate of MDS is ~4.5 cases per 100,000 people annually with a median age at diagnosis of around 70 years.[2] The genetically mutant clonal hematopoietic stem/progenitor cells (HSPCs) in MDS display defects in the generation of mature PB cells due to their impaired differentiation and survival.[3] The mutant HSPCs also induce an inflammatory bone marrow (BM) microenvironment, inhibiting hematopoiesis from the remaining healthy HSPCs.[4] Furthermore, mutant HSPCs exhibit a growth advantage over healthy HSPCs in inflammatory BM and predispose to secondary hits which lead to transformation to AML.[5] A better understanding of the pathogenesis of MDS and the development of novel effective targeted therapies are urgently required for these diseases. [6]

Despite showing normal to hypercellularity in BM, almost all MDS patients exhibit cytopenia due to the impaired production of mature blood cells. Studies suggested that this ineffective hematopoiesis is caused by the aberrant activation of innate immune signaling in BM hematopoietic cells (HCs) and its associated tendency toward programmed cell death (PCD) and inflammatory cytokine production.[4] Increased apoptosis, pyroptosis and necroptosis of BM HCs were reported independently by different studies to explain ineffective hematopoiesis in MDS.[7-9] We found that all three types of PCD can be detected in individual BM tissue of most MDS patients, specifically MDS with mutations in splicing factors *SF3B1* or *SRSF2*, suggesting PANoptosis.

PANoptosis is a collective term referring to all three types of PCD, pyroptosis, apoptosis and necroptosis, which can be induced by pathogen- and damage-associated molecular patterns (PAMPs and DAMPs) as well as combined stimulation from IFNγ and TNFα.[10] It has been described recently in some pathogen infections[11, 12] and has been implicated in the pathogenesis of some chronic inflammatory diseases and cancers.[13, 14] PANoptosis is mediated by a large multi-molecular complex called a PANoptosome, containing the key signaling components of all three types of PCD (ASC/NLRP3/CASP1/11 for pyroptosis, FADD/pro-CASP8 for apoptosis, RIPK1/RIPK3 for necroptosis). The PANoptosome provides a scaffold platform for the

intensive crosstalk among the three PCD pathways.[15] Caspase 8 (CASP8) functions as the "switch" among the three types of PCD.[15] TAK1, RIPK1 and IRF1 have been described as the master regulators of PANoptosis. In many situations, RIPK1 kinase activity is required for all three types of PCD.[11, 12, 15, 16]

Heterozygous missense mutations of *SF3B1* have been reported in ~20% of all MDS cases, and >80% of MDS patients with ring sideroblasts (RS).[17] Mutant *SF3B1* (*SF3B1*^{mut}) in HSPCs primarily affects erythropoiesis which causes refractory macrocytic anemia with RS, representing a distinct nosologic entity.[17] *SF3B1*^{mut} causes neomorphic function, resulting in the alternative use of cryptic splice sites of target transcripts. Aberrant splicing of a large number of transcripts has been identified in *SF3B1*^{mut} HSPCs[18]. Among them, mis-splicing of *Tmem14c* and *Abcb7* have been determined to be the causes of the RS phenotype.[19] However, the key driver(s) for macrocytic anemia has not been identified. Mis-splicing of *TAK1* has been consistently detected in both human and mouse *SF3B1*^{mut} HSPCs, resulting in nonsense-mediated decay of *TAK1* mRNA.[18]

To study the role of TAK1 in the pathogenesis of *SF3B1*^{mut} MDS, we knocked down *Tak1* (*Tak1*^{KD}) in HSPCs using shRNA. We found that mice which had received *Tak1*^{KD}-HSPCs developed macrocytic anemia, recapitulating the phenotype observed in *Sf3b1*$^{+/K700E}$ mice.[20, 21] Importantly, red blood cell (RBC) counts in such anemic mice can be restored by Ripk1 inhibition. Furthermore, *Tak1*^{KD}-HSPCs are hypersensitive to *Tak1* inhibitor or cIAP inhibitor treatment. Such treatments eliminate the *Tak1*^{KD}-HSPCs in animal models and human *SF3B1*^{mut}-HSPCs *in vitro*.

Methods

Mice. *Rosa26*^{CreErt}*Tak1* $^{fx/fx}$ mice and *Rosa26*^{CreErt}*Casp8*$^{fx/fx}$*Ripk3*$^{-/-}$ mice have been described previously. They were maintained in a C57BL/6J background.[22, 23] *Wild-type* (*WT*) C57BL/6J control mice and Ptprc recipient mice were purchased from The Jackson Laboratory (Bar Harbor, ME) and from GemPharmatech Co., Ltd., (Nanjing, China). All mice were maintained according to the standards of the National Institutes of Health *Guidelines for the Care and Use of Animals* in the AAALAC-certified pathogen-free animal facility at Loyola University Medical Center and

at Soochow University. All mice were housed under a 12-h. light/dark cycle in microisolator cages contained within a laminar flow system. All procedures were conducted in accordance with the National Institutes of Health guidelines for the care and use of laboratory animals for research purposes and were approved in advance by the Loyola University Chicago IACUC (AU 2020-011) or the Ethics Committee of Soochow University (SUDA20221214A02, Suzhou, China). Genotypes of mice were determined by PCR assay. The PCR primer sequences for genotyping can be found in **Table S1**. Please see supplementary information for more experimental procedures.

Results

Increased PANoptosis in MDS patient blood samples. To study whether PANoptosis is involved in the pathogenesis of MDS, we examined CASP3-apoptosis, NLRP3/ASC-pyroptosis and RIPK3/MLKL1-necroptosis in BM samples from 25 patients with low to intermediate-risk MDS (15 with *SF3B1*^{mut}, 6 with *SRSF2*^{mut} and 4 without spliceosome mutations) using flow cytometry. Five BM samples from patients with iron-deficiency anemia or folic acid deficiency anemia were studied as controls. To reduce the influence of dead cells/debris generated during the process of sample collection and freezing/thawing, prior to staining, we removed the dead cells/debris by density gradient centrifugation using Ficoll-Paque™ PLUS. We believe that the cells with positive PCD markers in our analysis were dying cells with activated death signals. We found that increased apoptosis (active CASP3^{+}), necroptosis (p-MLKL^{+}) and pyroptosis (ASC-speck^{+}) can be detected in all patient samples compared to control samples (**Figure 1a, b**). The PANoptosis was verified in 5 patients and 5 control samples by immunofluorescent co-staining of BM sections (**Figure 1c, d**). To further verify this data, we collected BM mononucleated cells (MNCs) from three *SF3B1*^{mut} MDS patients to assess TAK1 protein levels and activation of PANoptotic signaling using Western blotting. Compared to BM MNCs and CD34^{+} HSPCs from age-matched HDs, TAK1 levels are downregulated in all MDS patient samples (**Figures 1e, S1**), which are associated with increased RIPK1 activation as demonstrated by elevated p-Ser166 RIPK1. We also detected elevated apoptosis as displayed by the cleaved form of CASP8, necroptosis as shown by increased p-MLKL and pyroptosis as exhibited by

cleaved forms of CASP1 and GSDMD (**Figure 1e**). In addition, consistent with other reported findings[24], we found elevated activation of NFκB signaling in all three MDS samples. However, p38-MAKP signaling is significantly downregulated (**Figure 1e**). Moreover, we found elevated activation of TBK1 signaling in all three MDS samples.

Tak1 *knockdown in HSPCs induces PANoptosis.* In studying *Tak1*$^{-/-}$ mice, we and others have reported that Tak1 is required for the survival of adult HSPCs. Induced deletion of *Tak1* in mice causes massive death of HSPCs and acute BM failure.[23, 25] Complete depletion of hematopoietic progenitor cells was observed 2-3 days after *Tak1* deletion while complete exhaustion of HSCs occurred on days 5-6, suggesting that HSCs are relatively resistant to *Tak1* deletion-induced PCD compared to HPCs.[23, 26] Detailed analysis suggests that, in addition to PANoptosis, Tak1 may also protect HSPCs from lysosome-mediated cell death[27] because PCD in *Tak1*$^{-/-}$ HSPCs can only be partially prevented by Z-VAD-FMK (pan-Casp inhibitor) + Casp8/Ripk3 depletion, which can be further prevented by the addition of the cathepsin B inhibitor CA-074Me (**Figure S2**). Consistently, although BM hematopoiesis is largely normal in young *Tak1*$^{-/-}$*Casp8*$^{-/-}$*Ripk3*$^{-/-}$ mice, increased PCD of BM HCs is still detectable compared to age-matched control mice. Interestingly, Tak1 protein levels in *Tak1*$^{+/-}$ HSPCs are comparable to those in *WT* HSPCs.[23, 26] *Tak1*$^{+/-}$ mice are healthy and show a normal lifespan.

To study *Tak1* expression in BM cells, we purified different stages of HSPCs, committed progenitors and EBs from *WT* mice using FACS with the gating strategy described in[28] **Figure S3a, b**. *Tak1* expression was examined by TaqMan qRT-PCR. In BM HSPCs, *Tak1* expression was low in lin^{-}Sca1^{+}ckit^{+}CD150^{+}CD48^{-} HSCs and elevated during MPP (multipotent progenitor) and pre-GM differentiation and downregulated during further GMP (granulocyte-monocyte progenitors) and CD11b^{+}Ly6G^{+} granulocyte differentiation. Highest levels of *Tak1* were detected in pre-MegE (**Figure 2a**). During the erythroid differentiation of pre-MegE, *Tak1* was downregulated in early erythroid progenitor pre-CFU-E and then upregulated during further differentiation of EBs (**Figure 2b**). Aberrant splicing of 51-72% *TAK1* transcripts was detected in *SF3B1*^{mut} MDS patient cells.[24] To manipulate TAK1 downregulation in *SF3B1*^{mut} HSPCs, we transduced mouse HSPCs using a set of three different *shRNAs*, >70% reduced Tak1 mRNA and protein levels were detected in *sh2-Tak1* and *sh3-Tak1* transductions (**Figure 2c-d**). Annexin V^{+} is not specifically indicative of apoptosis; it is also positive in cells undergoing necroptosis or

pyroptosis. Compared to scrambled-*shRNA* (*Scr*)-transduced HSPCs, a significant increase in spontaneous PCD was detected in HSPCs transduced with *sh2-Tak1* and *sh3-Tak1* but not in HSPCs transduced with *sh1-Tak1* (**Figure S4a**). To determine the types of PCD, we transduced HSPCs from *WT* and *Casp8*$^{-/-}$*Ripk3*$^{-/-}$ mice with *sh2-Tak1* and *sh3-Tak1*. We found that the PCD of *sh2-Tak1* and *sh3-Tak1*-transduced HSPCs can be partially prevented by *Casp8*$^{-/-}$*Ripk3*$^{-/-}$ but is almost completely prevented by further addition of Z-VAD-FMK or VX-765 (Casp1/4 inhibitor) treatment, suggesting increased spontaneous PANoptosis of *sh2-Tak1*- and *sh3-Tak1*-HSPCs (**Figure 2e, S4b**). Furthermore, PCD of *sh2-Tak1*- and *sh3-Tak1*-HSPCs can be nearly completely prevented by Ripk1-specific inhibition (**Figure 2e, S4b**). However, unlike *Tak1*$^{-/-}$ HSPCs, the addition of CA-074Me failed to further prevent PCD of *sh2-Tak1*- and *sh3-Tak1*-HSPCs (**Figure S4c**). The PANoptosis of *sh2-Tak1* and *sh3-Tak1* HSPCs was further verified by Western blotting. As is the case with *SF3B1*^{mut} HSPCs[18], *sh2-Tak1* and *sh3-Tak1* HSPCs also displayed elevated p-Ser166 Ripk1, cleaved forms of Casp8 and Casp3, p-Mlkl and cleaved forms of Casp1 and Gsdmd (**Figure 2d, f**). *sh2-Tak1* and *sh3-Tak1* HSPCs also exhibited elevated Tbk1-NFκB signaling and reduced p38-Mapk signaling (**Figure 2g**).

Mice transplanted with Tak1*^{KD}*-HSPCs developed MDS-like diseases. To study the role of Tak1 in the pathogenesis of MDS, we treated *WT* C57Bl6/J mice with 10μg LPS and 125μg polyI:C, six times each, every other day, to induce aged-related BM changes.[29] Two weeks post treatment, we collected HSPCs from the BM and infected with *sh3-Tak1-GFP* virus or *scr-GFP* virus. Two days post-infection, the transduced HSPCs were purified by FACS for GFP$^+$ cells and expanded in HSC expansion medium. The HSPCs in both *sh3-Tak1*- and *scr*-groups were enriched with phenotypic HSCs and comparable at the time of collection (**Figure S5a**). Cells were then transplanted into lethally-irradiated mice (**Figure 3a**). We found that all mice that received *Tak1*^{KD}-HSPCs developed macrocytic anemia within 3-4 months of transplantation as demonstrated by reduction of RBC counts and hemoglobin (Hb) levels as well as increased mean corpuscular volume (MCV) of RBCs (**Figure 3b**). In addition, these mice showed neutrocytosis as demonstrated by increased white blood cells (WBC) due to the increased CD11b$^+$Ly6G$^+$ neutrophils (**Figure 3b & S5b**); however, platelets were less affected (**Figure 3b**). Nevertheless, the BM cellularity of mice which had received *Tak1*^{KD}-HSPCs was comparable to mice which had received *scr*-HSPCs (**Figure 3c**). At the time of analysis, >90% of PB WBCs and >80% of

BM MNCs were GFP$^+$ in mice that had received either *Tak1*^{KD}-HSPCs or *scr*-HSPCs (**Figure S5c**). EBs lost GFP expression during maturation, explaining why GFP$^+$ cell% was lower in BM compared to PB. Although GFP$^+$ cell% in *Tak1*^{KD}-group tended to be reduced, there was no significant difference compared to GFP$^+$ cell% in the *scr*-group. LKS$^+$ (lineage$^-$, c-Kit$^+$ and Sca1$^+$) HSPCs were slightly increased in the *Tak1*^{KD}-group, while LKS$^-$ (lineage$^-$, c-Kit$^+$ and Sca1$^-$) myeloid progenitors were comparable between the two groups (**Figure 3d**). Most importantly, >98% of HSPCs in both groups were GFP$^+$ (**Figure S5d**). HSCs and GMPs were increased while MPP4 and pre-MegEs were reduced in the *Tak1*^{KD}-group (**Figure 3e-f, S5e**). However, MPP1, MPP2, MPP3, pre-GMs and MkPs (megakaryocyte progenitors) were comparable between the two groups (**Figure S5e**). Although pre-CFU-E and CFU-E erythroid progenitors were moderately reduced in the *Tak1*^{KD}-group (**Figure 3f**), EBs were increased in the BM of the *Tak1*^{KD}-group (**Figure 3g**). Within EBs, the frequencies of R2-basophilic (Baso)-EBs and R3-polychromatophilic (poly)-EBs were reduced, while R4-orthochromatic (orth)-EBs were increased (**Figure 3h**), suggesting aberrant differentiation of EBs. The significantly increased PCD in c-Kit$^+$ HSPCs and c-Kit$^-$ HCs, specifically in EBs, suggested a critical role of PCD in the ineffective erythropoiesis (**Figure 3i**). The phenotype of *Tak1*^{KD}-mice seems to better resemble the reported phenotype of *Sf3b1*$^{+/K700E}$ mice.[20, 21]

After anemia had developed in mice transplanted with Tak1^{KD}-HSPCs, Ripk1 inhibition mitigated this condition. To study whether the inhibition of Ripk1 can restore RBC counts in MDS mice, we transplanted another batch of mice. After moderate anemia developed (Hb <10g/l), we randomly divided the mice into two groups. One group was treated with GNE684 (a murine Ripk1 inhibitor) twice daily for 30 days, the other group was treated with vehicle. Mice transplanted with *scr*-HSPCs were studied in parallel as controls. All mice were euthanized for hematopoietic analysis one day after the last treatment (**Figure 4a)**. We found that GNE684 treatment did not affect PB cell counts and BM hematopoiesis in mice transplanted with *scr*-HSPCs (**Figure 4**). However, GNE684 treatment corrected all PB and BM hematopoietic abnormalities observed in mice transplanted with *Tak1*^{KD}-HSPCs. Hb levels in vehicle-treated group were further reduced during treatment, while Hb levels in the GNE684 treatment group were significantly increased as early as 1 week of the treatment (**Figure 4b)**, which were associated with correction of WBC, RBC and MCV (**Figure S6a)**. At 1 month of treatment, >90%

of PB WBCs and >80% of BM MNCs in all groups of mice were GFP^+ and comparable (**Figure S6b**). PB cell counts in GNE684 treated *Tak1*^{KD}-group were restored to the levels of *scr*-controls (**Figure 4c**). In BM, the differentiation defect of EBs (**Figures 4d-e)** as well as alterations of erythroid progenitors (**Figures 4f)** and HSPCs (**Figures 4g, S6c-d)** were largely corrected in the GNE684-treated group. The increased PCD of HCs, HSPCs and EBs was inhibited in the GNE684-treated group (**Figure 4h)**.

To study whether the premature differentiation of *Tak1*^{KD}-EBs is related to premature downregulation of Gata1 as described in *SF3B1*^{mut}-EBs[24], we cultured *Tak1*^{KD}- and *scr*-HSPCs in a two-phase *in vitro* erythropoiesis system. After 6 days of expansion, the cells were transferred into differentiation medium for further incubation. Cells were collected after 12, 24 and 48 hours of culturing for analysis. We found that Gata1 was downregulated as early as 24 hours in *Tak1*^{KD}-EBs, which was significantly earlier than Gata1 downregulation in *scr*-EBs (**Figure S6e)**. However, the differentiation stages of *Tak1*^{KD}-EBs at 24 hours of culture were comparable to those of *scr*-EBs (**Figure S6f)**, suggesting premature Gata1 downregulation. The premature downregulation of Gata1 could be prevented by Ripk1 inhibition, and Ripk3/Casp8 inhibition (**Figure S6g)**, suggesting a Ripk1-Ripk3/Casp8-dependent mechanism of Gata1 downregulation. In addition, the elevated NFκB signaling in *Tak1*^{KD}-HSPCs can also be repressed by Ripk1 inhibition and Tbk1 inhibition, implicating a Ripk1-Tbk1 axis-mediated NFκB activation (**Figure S6h)**.

Tak1^{KD}-*HSPCs are sensitive to Tak1 inhibitor and cIAP inhibitor treatment.* We speculate that *Tak1*^{KD}-HSPCs rely on residual Tak1 activity for their survival, and Tak1 inhibition might induce synthetic lethality in *Tak1*^{KD}-HSPCs. We treated *Tak1*^{KD}-HSPCs and *scr*-HSPCs with the cIAP inhibitor birinapant or the Tak1 inhibitor HS-276. In mixed suspension culture of transduced and no-transduced HSPCs (**Figure 5a)**, both birinapant and HS-276 preferentially killed *Tak1*^{KD}-HSPCs with reduced effect on *scr*-HSPCs as demonstrated by significantly reduced the percentage of *Tak1*^{KD}-HSPCs (**Figure 5b)**. In methylcellulose clonal assays, both birinapant and HS-276 treatment yielded significantly reduced the clone-forming ability of *Tak1*^{KD}-HSPCs with reduced effect on *scr*-HSPCs (**Figure 5c)**. To study inhibition of Tak1 signaling on *Tak1*^{KD}-HSPCs *in vivo*, we transplanted a mixture of *Tak1*^{KD}-HSPCs and normal HSPCs into recipient mice. Thirty days after transplantation and following an examination of the percentages of PB

contributions of *Tak1*^{KD}-HSPCs, the recipient mice were randomly divided into three groups. Mice in groups 1 and 2 were treated with HS-276 and birinapant, respectively, while mice in group 3 were treated with vehicle (**Figure 5a)**. We found that HS-276 and birinapant treatment did not affect the PB and BM contribution of *scr*-HSPCs but largely eliminated the *Tak1*^{KD}-HSPC-derived cells in the recipient animals as demonstrated by a significant reduction of GFP$^+$ % in PB and BM (**Figure 5d-e**). When analyzed 2 months after HS-276 and birinapant withdrawal, blood cell counts in HS-276 and birinapant-treated groups remained normal (**Figure S7a**) and were primarily replenished by GFP$^-$ normal HSPCs (**Figure S7b**). However, the RBC counts and Hb levels in the vehicle-treated mice were slightly lower than in control group mice (**Figure S7a**).

RIPK1 inhibition restored the proper growth of* SF3B1^{mut}*-EBs from MDS patients. *SF3B1*^{mut}-MDS HSPCs displayed a reduced clone-forming ability and late erythroid differentiation defect[24, 30] (**Figure 6a**). We seeded BM MNCs from *SF3B1*^{mut}-MDS patients for CFU assay with or without RIPK1 inhibitor GSK3145095 treatment. We found that GSK3145095 did not affect the colony-forming capacity of HSPCs from HDs but increased colony-forming capacity of *SF3B1*^{mut}-MDS HSPCs (**Figure 6a**). To study whether inhibition of RIPK1 can restore survival and normal differentiation to *SF3B1*^{mut}-HSPCs, we isolated CD34$^+$ HSPCs from BM of MDS patients and HDs. Using the 3-phase erythroid culture system with medium change every-other day[31] (**Figure 6b**), GSK3145095 or vehicle were added during medium changes. Compared to HSPCs from five HDs, HSPCs from all five MDS samples produced significantly fewer cells during 14 days of culturing (**Figure 6c**). Although comparable numbers of BFU-E and CFU-E were produced by MDS-HSPCs and HD-HPSCs by day 7 of expansion culture, a significant reduction of Pro-EB was observed in the MDS culture (**Figure 6d, S8a**). When examined on day 14, a significantly fewer number of late-Baso-EBs, poly-EBs, Ortho-EBs and reticulocytes (Rets) were detected in MDS culture (**Figure 6e, f, S8a-b**).[32] GSK3145095 treatment affected neither the expansion of BFU-E/CFU-E nor the differentiation of HD-EBs; however, GSK3145095 treatment significantly enhanced the production of EBs and Rets of MDS-HSPCs (**Figure 6c-f**). The reduced production of EBs and Rets of MDS-HSPCs was most likely due to the increased RIPK1-dependent PCD and late differentiation blockage because both can be largely reversed by GSK3145095 treatment (**Figure 6e, g**).

Tak1 inhibitor treatment preferentially killed* SF3B1^{mut}*-HSPCs. To study whether TAK1 inhibitor treatment can induce synthetic lethality in *SF3B1^{mut}*-HSPCs, we isolated CD34^{+} HSPCs from MDS patients and HDs. The HSPCs were incubated in Soluplus-based 4a-HSPC expansion medium and treated with 10μM of HS-276. Cells were collected on day 3 of culturing for RIPK1 and p-RIPK1 protein level analysis, day 4 for cell death analysis, and day 6 for live-cell counts and targeted DNA-seq to detect mutational variant allele frequency (VAF) of the *SF3B1^{mut}* genes (**Figure 6h**). In the vehicle-groups, p-RIPK1 levels and cell death were higher in MDS HSPCs compared to HD HSPCs (**Figures 6i, S9a-b**). HS276 treatment tends to induce p-RIPK in HD HSPCs but triggers much higher p-RIPK1 levels in MDS HSPCs (**Figures 6i, S9a**). Consistently, we found a more significant increase in PCD in MDS HSPCs compared to HD-HSPCs after HS276 treatment (**Figures 6j, S9b**) which resulted in a significant reduction of live cells in MDS samples (**Figure S9c**). VAF analysis of mutant genes demonstrated that HS-276 treatment significantly reduced *SF3B1^{mut}*-HSPCs (**Figure 6k**).

Discussion

Increased PCD and blockage of terminal erythroid differentiation of EBs are believed to be the major causes of ineffective erythropoiesis observed in *SF3B1^{mut}*-MDS patients.[17, 33] Mis-splicing of TAK1 is always detected in *SF3B1^{mut}* cells, which leads to nonsense decay of *TAK1* mRNA.[18, 24] Our study suggests that TAK1 down-regulation is the major cause of ineffective erythropoiesis in *SF3B1^{mut}*-MDS patients. We found TAK1-downregulation and increased spontaneous PANoptosis in BM samples of *SF3B1^{mut}*-MDS patients. *Tak1*-downregulation results in Ripk1 overactivation and spontaneous PANoptosis in mouse HSPCs. In both murine *Tak1^{KD}*-HSPCs and human *SF3B1^{mut}*-HSPCs, the inhibition of RIPK1 can prevent PANoptosis and correct the differentiation defects of EBs. Furthermore, both human *SF3B1^{mut}*-HSPCs and murine *Tak1^{KD}*-HSPCs are hypersensitive to the inhibition of TAK1 signaling. Our study suggests that *SF3B1^{mut}*-MDS can be treated by either inhibition of RIPK1-PANoptosis to restore normal erythropoiesis or by inhibition of TAK1 signaling to induce synthetic lethality of the mutant HSPCs.

RIPK1 over-activation not only promotes spontaneous PANoptosis of EBs but also induces aberrant differentiation of EBs. Consistent with the findings of Lieu *et al.*,[24] we found that the aberrant differentiation of *Tak1*^{KD}-EBs is associated with premature downregulation of Gata1. Lieu *et al*. proposed that TAK1 downregulation promotes the proteasomal degradation of GATA1 via the p38-MK2/HSP27 pathway.[24, 34] In fact, downregulation of p38-MK2 signaling can also cause RIPK1 activation.[35, 36] We found that the premature downregulation of Gata1 in *Tak1*^{KD}-EBs is largely mediated by Ripk1-Casp8 signaling. Although Casp8 cannot directly cleave Gata1, it activates Casp3 and Casp1, both of which can cleave Gata1.[37, 38] Thus, both spontaneous PANoptosis and the premature differentiation defects of *Tak1*^{KD}- or *Sf3b1*$^{+/K700E}$-EBs can be reversed by Ripk1 inhibition. Many RIPK1-specific inhibitors have been developed. Several of them have been evaluated in clinical trials for autoimmune and neuroinflammatory diseases, and have shown excellent safety and promising results.[39] Therefore, it will be important to test whether RIPK1 inhibition can mitigate the anemia that is so common in *SF3B1*^{mut}-MDS patients.

In normal HCs, PANoptosis is restricted by TAK1 signaling. TAK1 signaling is normally activated by PAMPs, DAMPs and inflammatory cytokines.[40, 41] TAK1 and its downstream signaling mediators IKKs/NEMO and MK2 limit RIPK1-dependent PANoptosis by phosphorylating RIPK1.[39] cIAP1/2 and LUBAC, the upstream mediators of TAK1 signaling, also repress RIPK1-dependent PANoptosis by mediating K63- and M1-linked ubiquitination of RIPK1.[42] In BM-derived macrophages (BMDMs), *Tak1*$^{-/-}$ induces spontaneous Ripk1-dependent PANoptosis.[43] TAK1 signaling also restricts RIPK1-independent PANoptosis by regulating NFκB-mediated the expression of several pro-survival genes. BMDMs deficient in *Tak1* are hypersensitive to LPS or polyI:C-induced Ripk1-dependent and -independent PANoptosis.[44] However, all of our experiments were performed in a specific pathogen-free environment without any PAMP challenges. Future study needs to determine whether Ripk1 inhibitor treatment can also mitigate anemia in mice with *Tak1*^{KD}-HSPCs or *Sf3b1*$^{+/K700E}$-HSPCs in a pathogen infection setting. In addition, we used LPS/polyI:C pre-treated BM HSPCs in our transduction studies. Although LPS/polyI:C pre-treatment only induces age-like epigenetic/metabolic memory in BM HSPCs without increasing genetic mutations[29], it is not known whether *Tak1*^{KD} in HSPCs from untreated young or old mice can also induce MDS-like

disease. Furthermore, future study needs to elucidate why *Tak1*^{KD} in HSPCs primarily affects certain stages of EBs.

In most types of tissue cells, TAK1 inactivation is always associated with NFκB signaling inhibition.[40] However, in *SF3B1*^{mut}-HSPCs, NFκB signaling activity is enhanced.[18] We found that such TAK1-independent NFκB signaling activation is most likely due to the overactivation of RIPK1-TBK1 signaling. In addition to activating PANoptosis, activated RIPK1 can also activate TBK1-dependent IFNα/β [22, 45] and NFκB signaling.[46] Activated RIPK1 can also translocate to the nucleus to promote the expression of *NFκB* target genes by recruiting a BAF complex to enhancers/promotors.[47] Therefore, active RIPK1 might promote NFκB signaling activity via both TBK1-mediated regulation and BAF complex-mediated tight gene expression.

We found that TAK1 is downregulated in BM HCs from patients with *SF3B1*^{mut}-MDS, while dysregulation of other master regulators of the PANoptotic pathway have been reported in MDS patients with other genetic mutations. For example, mutations of *SRSF2* cause mis-splice of *CASP8*.[18] Down-regulating CASP8 results in hypersensitivity of cells to necroptosis and pyroptosis due to elevated RIPK1 protein levels.[15] In low-grade MDS patients, downregulation of CASP8 and increased RIPK1 protein are detected in BM HCs.[48] *Ripk1* overexpression or *Casp8* knockout in HSPC induces PCD and MDS-like disease in mice.[9, 22] Thus, targeting PANoptotic signaling might also be a useful strategy for treating MDS with other genetic mutations.

Although increased PCD is commonly detected in HCs from MDS patients, the number of HSPCs in MDS patients is not reduced, most likely due to inflammatory cytokine-stimulated compensatory proliferation. Cells which die of PANoptosis produce inflammatory cytokines such as TNFα and IL1β. TNFα and IL1β induce PCDs and differentiation in myeloid progenitor cells[49, 50]. However, owing to the higher-level expression of pro-survival genes such as cIAP2, HSCs are relatively resistant to inflammatory cytokine-induced PCD[49]. Currently, we are developing more sensitive assays for the detection of PANoptosis. We want to determine which cell populations in MDS patient BM are undergoing PANoptosis. We also want to distinguish whether all three types of PCD occur in the same cells *vs*. different cell types.

References

1. Sekeres MA, Taylor J. Diagnosis and Treatment of Myelodysplastic Syndromes: A Review. JAMA. 2022;328(9):872-880.
2. McQuilten ZK, Wood EM, Polizzotto MN, et al. Underestimation of myelodysplastic syndrome incidence by cancer registries: Results from a population-based data linkage study. Cancer. 2014;120(11):1686-1694.
3. Nazha A, Sekeres MA, Bejar R, et al. Genomic Biomarkers to Predict Resistance to Hypomethylating Agents in Patients With Myelodysplastic Syndromes Using Artificial Intelligence. JCO Precis Oncol. 2019;3:PO.19.00119.
4. Sallman DA, List A. The central role of inflammatory signaling in the pathogenesis of myelodysplastic syndromes. Blood. 2019;133(10):1039-1048.
5. Vallelonga V, Gandolfi F, Ficara F, et al. Emerging Insights into Molecular Mechanisms of Inflammation in Myelodysplastic Syndromes. Biomedicines. 2023;11(10):2613.
6. Steensma DP. Graphical representation of clinical outcomes for patients with myelodysplastic syndromes. Leuk Lymphoma. 2016;57(1):17-20.
7. Parker JE, Mufti GJ, Rasool F, et al. The role of apoptosis, proliferation, and the Bcl-2-related proteins in the myelodysplastic syndromes and acute myeloid leukemia secondary to MDS. Blood. 2000;96(12):3932-3938.
8. Basiorka AA, McGraw KL, Eksioglu EA, et al. The NLRP3 Inflammasome functions as a driver of the myelodysplastic syndrome phenotype. Blood. 2016;128(25):2960-2975.
9. Wagner PN, Shi Q, Salisbury-Ruf CT, et al. Increased Ripk1-mediated bone marrow necroptosis leads to myelodysplasia and bone marrow failure in mice. Blood. 2019;133(2):107-120.
10. Sharma BR, Karki R, Rajesh Y, et al. Immune regulator IRF1 contributes to ZBP1-, AIM2-, RIPK1-, and NLRP12-PANoptosome activation and inflammatory cell death (PANoptosis). J Biol Chem. 2023;299(9):105141.
11. Sundaram B, Pandian N, Mall R, et al. NLRP12-PANoptosome activates PANoptosis and pathology in response to heme and PAMPs. Cell. 2023;186(13):2783-2801 e2720.
12. Lee S, Karki R, Wang Y, et al. AIM2 forms a complex with pyrin and ZBP1 to drive PANoptosis and host defence. Nature. 2021;597(7876):415-419.
13. Qi Z, Zhu L, Wang K, et al. PANoptosis: Emerging mechanisms and disease implications. Life Sci. 2023;333:122158.
14. Cai H, Lv M, Wang T. PANoptosis in cancer, the triangle of cell death. Cancer Med. 2023;12(24):22206-22223.
15. Christgen S, Zheng M, Kesavardhana S, et al. Identification of the PANoptosome: A Molecular Platform Triggering Pyroptosis, Apoptosis, and Necroptosis (PANoptosis). Front Cell Infect Microbiol. 2020;10:237.
16. Malireddi RKS, Kesavardhana S, Kanneganti TD. ZBP1 and TAK1: Master Regulators of NLRP3 Inflammasome/Pyroptosis, Apoptosis, and Necroptosis (PAN-optosis). Front Cell Infect Microbiol. 2019;9:406.
17. Malcovati L, Stevenson K, Papaemmanuil E, et al. SF3B1-mutant MDS as a distinct disease subtype: a proposal from the International Working Group for the Prognosis of MDS. Blood. 2020;136(2):157-170.

18. Lee SC, North K, Kim E, et al. Synthetic Lethal and Convergent Biological Effects of Cancer-Associated Spliceosomal Gene Mutations. Cancer Cell. 2018;34(2):225-241.e228.
19. Clough CA, Pangallo J, Sarchi M, et al. Coordinated missplicing of TMEM14C and ABCB7 causes ring sideroblast formation in SF3B1-mutant myelodysplastic syndrome. Blood. 2022;139(13):2038-2049.
20. Mupo A, Seiler M, Sathiaseelan V, et al. Hemopoietic-specific Sf3b1-K700E knock-in mice display the splicing defect seen in human MDS but develop anemia without ring sideroblasts. Leukemia. 2017;31(3):720-727.
21. Obeng EA, Chappell RJ, Seiler M, et al. Physiologic Expression of Sf3b1(K700E) Causes Impaired Erythropoiesis, Aberrant Splicing, and Sensitivity to Therapeutic Spliceosome Modulation. Cancer Cell. 2016;30(3):404-417.
22. Liu S, Joshi K, Zhang L, et al. Caspase 8 deletion causes infection/inflammation-induced bone marrow failure and MDS-like disease in mice. Cell Death Dis. 2024;15(4):278.
23. Tang M, Wei X, Guo Y, et al. TAK1 is required for the survival of hematopoietic cells and hepatocytes in mice. J Exp Med. 2008;205(7):1611-1619.
24. Lieu YK, Liu Z, Ali AM, et al. SF3B1 mutant-induced missplicing of MAP3K7 causes anemia in myelodysplastic syndromes. Proc Natl Acad Sci U S A. 2022;119(1):e2111703119.
25. Takaesu G, Inagaki M, Takubo K, et al. TAK1 (MAP3K7) signaling regulates hematopoietic stem cells through TNF-dependent and -independent mechanisms. PLoS One. 2012;7(11):e51073.
26. Xiao Y, Li H, Zhang J, et al. TNF-alpha/Fas-RIP-1-induced cell death signaling separates murine hematopoietic stem cells/progenitors into 2 distinct populations. Blood. 2011;118(23):6057-6067.
27. Sakamachi Y, Morioka S, Mihaly SR, et al. TAK1 regulates resident macrophages by protecting lysosomal integrity. Cell Death Dis. 2017;8(2):e2598.
28. Liu J, Zhang J, Ginzburg Y, et al. Quantitative analysis of murine terminal erythroid differentiation in vivo: novel method to study normal and disordered erythropoiesis. Blood. 2013;121(8):e43-49.
29. Yokomizo-Nakano T, Hamashima A, Kubota S, et al. Exposure to microbial products followed by loss of Tet2 promotes myelodysplastic syndrome via remodeling HSCs. J Exp Med. 2023;220(7):e20220962.
30. DeZern AE, Pu J, McDevitt MA, et al. Burst-forming unit-erythroid assays to distinguish cellular bone marrow failure disorders. Exp Hematol. 2013;41(9):808-816.
31. Hu J, Liu J, Xue F, et al. Isolation and functional characterization of human erythroblasts at distinct stages: implications for understanding of normal and disordered erythropoiesis in vivo. Blood. 2013;121(16):3246-3253.
32. Yan H, Ali A, Blanc L, et al. Comprehensive phenotyping of erythropoiesis in human bone marrow: Evaluation of normal and ineffective erythropoiesis. Am J Hematol. 2021;96(9):1064-1076.
33. Fenaux P, Platzbecker U, Mufti GJ, et al. Luspatercept in Patients with Lower-Risk Myelodysplastic Syndromes. N Engl J Med. 2020;382(2):140-151.

34. de Thonel A, Vandekerckhove J, Lanneau D, et al. HSP27 controls GATA-1 protein level during erythroid cell differentiation. Blood. 2010;116(1):85-96.
35. Dondelinger Y, Delanghe T, Rojas-Rivera D, et al. MK2 phosphorylation of RIPK1 regulates TNF-mediated cell death. Nat Cell Biol. 2017;19(10):1237-1247.
36. Menon MB, Gropengiesser J, Fischer J, et al. p38(MAPK)/MK2-dependent phosphorylation controls cytotoxic RIPK1 signalling in inflammation and infection. Nat Cell Biol. 2017;19(10):1248-1259.
37. Tyrkalska SD, Perez-Oliva AB, Rodriguez-Ruiz L, et al. Inflammasome Regulates Hematopoiesis through Cleavage of the Master Erythroid Transcription Factor GATA1. Immunity. 2019;51(1):50-63.e5.
38. Ribeil JA, Zermati Y, Vandekerckhove J, et al. Hsp70 regulates erythropoiesis by preventing caspase-3-mediated cleavage of GATA-1. Nature. 2007;445(7123):102-105.
39. Li W, Yuan J. Targeting RIPK1 kinase for modulating inflammation in human diseases. Front Immunol. 2023;14:1159743.
40. Xu YR, Lei CQ. TAK1-TABs Complex: A Central Signalosome in Inflammatory Responses. Front Immunol. 2020;11:608976.
41. Mihaly SR, Ninomiya-Tsuji J, Morioka S. TAK1 control of cell death. Cell Death Differ. 2014;21(11):1667-1676.
42. Annibaldi A, Wicky John S, Vanden Berghe T, et al. Ubiquitin-Mediated Regulation of RIPK1 Kinase Activity Independent of IKK and MK2. Mol Cell. 2018;69(4):566-580.e5.
43. Malireddi RKS, Gurung P, Mavuluri J, et al. TAK1 restricts spontaneous NLRP3 activation and cell death to control myeloid proliferation. J Exp Med. 2018;215(4):1023-1034.
44. Malireddi RKS, Gurung P, Kesavardhana S, et al. Innate immune priming in the absence of TAK1 drives RIPK1 kinase activity-independent pyroptosis, apoptosis, necroptosis, and inflammatory disease. J Exp Med. 2020;217(3):jem.20191644.
45. Wang Y, Karki R, Mall R, et al. Molecular mechanism of RIPK1 and caspase-8 in homeostatic type I interferon production and regulation. Cell Rep. 2022;41:111434.
46. Runde AP, Mack R, Breslin JP, et al. The role of TBK1 in cancer pathogenesis and anticancer immunity. J Exp Clin Cancer Res. 2022;41(1):135.
47. Li W, Shan B, Zou C, et al. Nuclear RIPK1 promotes chromatin remodeling to mediate inflammatory response. Cell Res. 2022;32(7):621-637.
48. Zou J, Shi Q, Chen H, et al. Programmed necroptosis is upregulated in low-grade myelodysplastic syndromes and may play a role in the pathogenesis. Exp Hematol. 2021;103:60-72.e5.
49. Yamashita M, Passegue E. TNF-alpha Coordinates Hematopoietic Stem Cell Survival and Myeloid Regeneration. Cell Stem Cell. 2019;25(3):357-372.7.
50. Pietras EM, Mirantes-Barbeito C, Fong S, et al. Chronic interleukin-1 exposure drives haematopoietic stem cells towards precocious myeloid differentiation at the expense of self-renewal. Nat Cell Biol. 2016;18(6):607-618.

Figure legends

Figure 1. ***Increased spontaneous PANoptosis in MDS BM HCs***. **a-b**. Representative flow cytometric plots for p-MLKL, a(active)-CASP3 and ASC-speck analysis in MDS and control BM samples (**a**) and quantitated in **b**.*stands for $p<0.05$ compared to the other two MDS groups. **c-d**. Representative immune staining of p-MLKL, a(active)-CASP3 and ASC-speck in MDS BM samples (**c**) and quantitated in **d**. **e**. Western blotting analysis of TAK1 and CASP8 as well as PANoptotic and TBK1-NFκB signaling in MDS patient BM MNCs with *SF3B1* mutations compared to BM MNCs from age-matched healthy donors.

Figure 2. ***Increased PANoptosis in Tak1^{KD} HSPCs***. **a-b**. Indicated populations of HSPCs, erythroid precursors and EBs were isolated from BM of *WT* mice. *Tak1* mRNA expression was examined by quantitative RT-PCR. Triplicate experiments were conducted. ** indicates $p<0.01$ compared to HSCs in **a** and pre-MegE in **b**. **c-d**. c-Kit$^+$ HSPCs from *WT* mice were transduced with 3 shRNAs for *Tak1*, respectively. Cells were collected on day two of transduction for analysis. Scrambled shRNA (Scr) transduction was studied in parallel as a control. Relative *Tak1* expression was evaluated by RT-PCR. Triplicate experiments were conducted (**c**). ** indicates $p<0.01$ compared to Scr control. Western blot analysis of Tak1 and Casp8 (**d**). **e**. c-Kit$^+$ HSPCs from *WT* and *Casp8$^{-/-}$Ripk3$^{-/-}$* mice were transduced with *sh2Tak1* or *Scr*. One day post-transduction, after determining the transduction efficiency (GFP$^+$ cells %), cells were treated with 20μM pan-Casp inhibitor (Z-VAD) or 20μM Ripk1 inhibitor (Nec1s) daily. The relative rate of PCD of the *Tak1^{KD}* HSPCs was evaluated by detecting the GFP$^+$% every 2 days. Vehicle treatments (veh) were studied in parallel as controls. Triplicate experiments were conducted. ** indicates $p<0.01$. **f-g**. c-Kit$^+$ HSPCs from *WT* mice were transduced with 2 shRNAs for *Tak1*, respectively. Western blotting analysis of PANoptotic signaling (**f**), as well as Tbk1, NFκB, Jnk and p38 signaling (**g**) in s*hTak1* HSPCs compared to *scr*-HSPCs.

Figure 3. ***Mice transplanted with* Tak1^{KD} *HSPCs developed MDS-like diseases*** **a**. Schematic diagram of experimental procedures. Four months post-transplantation of *scr*-HSPCs and *Tak1^{KD}* HSPCs, PB cell counts were examined using a Hemavet (**b**). **c-i.** BM were collected, MNCs (**c**), LKS$^-$ myeloid progenitors and LSK$^+$ HSPCs (**d**), HSCs and MPP4s (**e**), pre-MegEs, pre-CFU-Es and CFU-Es (**f**), as well as EBs including R1-pro-EBs, R2- Baso-EBs, R3-poly-EBs and R4-orth-EBs (**g, h**) were analyzed by flow cytometry. PCD of cKit$^+$ HSPCS, cKit$^-$ HCs and Syto16$^+$Ter119$^+$ EBs were analyzed by flow cytometry for annexin-V (**i**).

Figure 4. ***Ripk1 inhibition restores normal BM hematopoiesis and blood cell counts in anemic Tak1^{KD} mice.*** **a**. Schematic diagram of experimental procedures. **b-g**. After anemia developed (Hb<10g/dl), the mice were randomly separated into two groups and treated with vehicle or GNE684, respectively, for one month. scr-HSPC transplantations were studied in parallel as controls. PB hemoglobin levels were analyzed on one day before the treatment (0) as well as at 1 and 2 weeks during the treatment (**b**). One day after the last treatment, mice were sacrificed

for hematopoietic analysis. PB cell counts were analyzed using a Hemavet (**c**). The percentages of EBs (**d**) and different differentiation stages of EBs in BM (**e**), absolute numbers of pre-MegE and erythroid progenitors (**f**), and absolute numbers of HSCs and MPP4 (**g**) in BM were analyzed by follow cytometry. The percentages of PCD of c-Kit$^-$ HCs, c-Kit$^+$ HSPCs and Syto16$^+$CD71$^{+/lo}$Ter119$^+$ EBs were examined by flow cytometric analysis of Annexin-V staining (**h**). * and ** indicate $p<0.05$ and $p<0.01$, respectively. ns indicates no significance.

Figure 5. Tak1 inhibitor or cIAP-inhibitor treatment induces synthetic lethality in* Tak1^{KD} *HSPCs. **a**. Schematic diagram of experimental procedures. **b**. *sh2Tak1-GFP*-transduced HSPCs (*Tak1^{KD}*) were mixed with untransduced HSPCs in a 1:1 ratio and treated with vehicle, Tak1 inhibitor HS-276 or cIAP-inhibitor birinapant. New chemicals were added on day two during medium change. The reduction of the transduced HSPCs was examined by analyzing the GFP$^+$ cell percentage. scr-GFP transduced HSPCs were studied in parallel as controls. **c.** *Tak1^{KD}* - and *scr*-transduced HSPCs were seeded for CFU assay and treated with vehicle, HS-276 or birinapant. CFU numbers were counted on day 7 of culturing. Three biological replicates were performed for data in **b** and **c**. **d-e**. *Tak1^{KD}* HSPCs (GFP$^+$) were mixed with non-transduced HSPCs in a 1.5:1 ratio, whereas *scr*- GFP transduced HSPCs were mixed with non-transduced HSPCs in a 1:1 ratio. The mixed HSPCs were transplanted into lethally-radiated mice. One-month post-transplantation, after determining the engraftment (GFP$^+$ cells in PB) of the transduced HSPCs, mice were divided into three groups and treated with vehicle, HS-276 or birinapant, respectively, for two weeks. The percentages of transduced cells in PB (**d**) were examined on days 7 and 14, and in BM were examined on day 14 (**e**). ** indicates $p<0.01$. ns indicates no significance.

Figure 6. Inhibition of RIPK1 and TAK1 in human SF3B1^{mut} MDS samples. **a**. BM cells from MDS patients and HDs were seeded into M3343 medium for CFU assay with or without RIPK1 inhibitor GSK3145095 treatment. CFU-Es were counted on day 7 of culturing and BFU-E, CFU-G/M and CFU-GMEM were counted on day 14 of culturing. **b**. Schematic diagram of experimental procedures for **c**-**g**. CD34$^+$ HSPCs from HDs or MDS patients were cultured in 3-phase erythroid culture system with or without GSK3145095 treatment. Cells were collected on days 7 and 14 of culturing; the numbers of cultured cells were plotted in the growth curve (**c**); BFU-E, CFU-E, Pro-EBs and early Baso-EBs were analyzed by flow cytometry on day 7 (**d**); late Baso-EBs, poly-EBs and ortho-EBs (**e**) and Rets (**f**) were analyzed by flow cytometry on day 14. PCD was analyzed on days 7 and 14, respectively, by examining Annexin-V$^+$ cells (**g**). **h**. Schematic diagram of experimental procedure for **i-k**. CD34$^+$ HSPCs from HDs or MDS patients were cultured in HSPC culture system with or without TAK1 inhibitor HS-276 treatment. Cells were collected on day 3 of culturing for analysis of RIPK1 and p-RIPK1 protein level by

flow cytometry (**i**), day 4 for cell death analysis by annexin-V/PI staining (**j**), and day 6 for targeted DNA sequencing (**k**). Mean fluorescence intensity (MFI) of RIPK1 and p-RIPK1 staining (**i**), and percentage of annexin-V^+ cells (**j**) were presented. The VAFs of mutant genes are presented in the Table (**k**). ns states for no significance.

Figure 1.

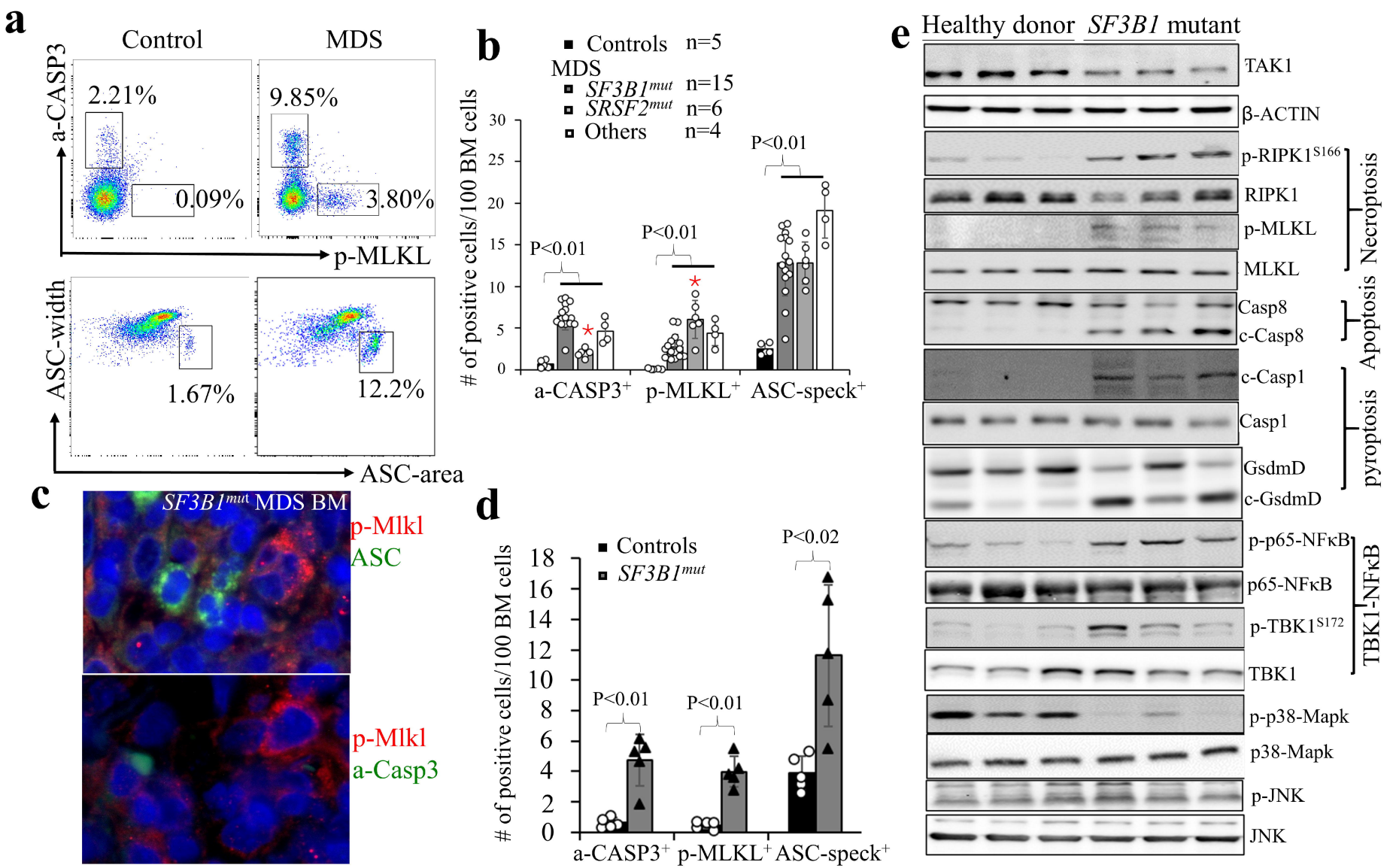
a
Control
MDS
a-CASP3
2.21%
0.09%
9.85%
3.80%
p-MLKL
ASC-width
1.67%
12.2%
ASC-area
b
Controls n=5
MDS
SF3B1mut n=15
SRSF2mut n=6
Others n=4
# of positive cells/100 BM cells
P<0.01
P<0.01
P<0.01
a-CASP3+
p-MLKL+
ASC-speck+
c
SF3B1mut MDS BM
p-Mlkl
ASC
p-Mlkl
a-Casp3
d
Controls
SF3B1mut
# of positive cells/100 BM cells
P<0.01
P<0.01
P<0.02
a-CASP3+
p-MLKL+
ASC-speck+
e
Healthy donor
SF3B1 mutant
TAK1
β-ACTIN
p-RIPK1S166
RIPK1
p-MLKL
MLKL
Necroptosis
Casp8
c-Casp8
Apoptosis
c-Casp1
Casp1
GsdmD
c-GsdmD
pyroptosis
p-p65-NFκB
p65-NFκB
p-TBK1S172
TBK1
TBK1-NFκB
p-p38-Mapk
p38-Mapk
p-JNK
JNK

Figure 2

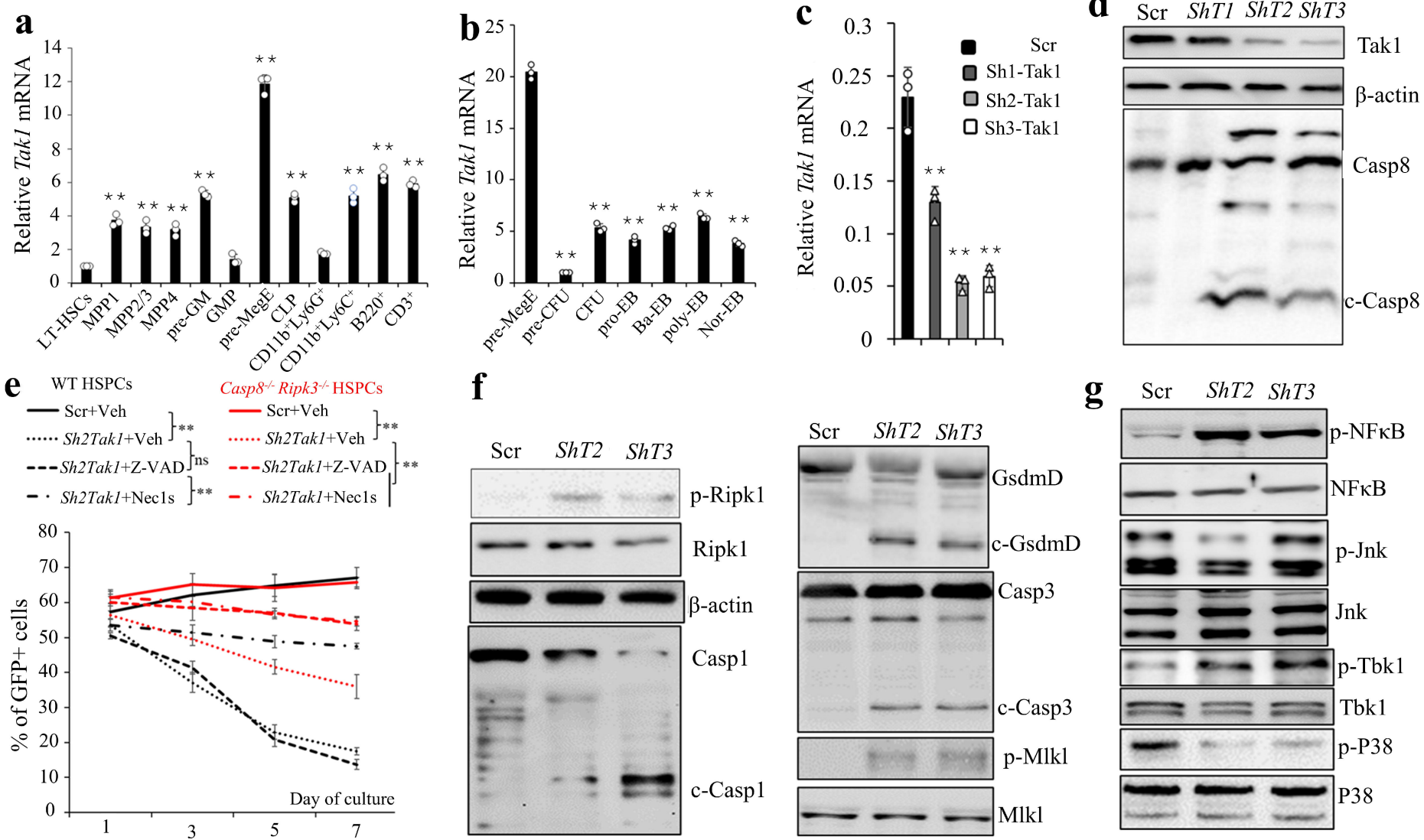
a
Relative Tak1 mRNA
LT-HSCs
MPP1
MPP2/3
MPP4
pre-GM
GMP
pre-MegE
CLP
CD11b+Ly6G+
CD11b+Ly6C+
B220+
CD3+
b
Relative Tak1 mRNA
pre-MegE
pre-CFU
CFU
pro-EB
Ba-EB
poly-EB
Nor-EB
c
Relative Tak1 mRNA
Scr
Sh1-Tak1
Sh2-Tak1
Sh3-Tak1
d
Scr
ShT1
ShT2
ShT3
Tak1
β-actin
Casp8
c-Casp8
e
WT HSPCs
Casp8-/- Ripk3-/- HSPCs
Scr+Veh
Sh2Tak1+Veh
Sh2Tak1+Z-VAD
Sh2Tak1+Nec1s
ns
% of GFP+ cells
Day of culture
f
Scr
ShT2
ShT3
p-Ripk1
Ripk1
β-actin
Casp1
c-Casp1
GsdmD
c-GsdmD
Casp3
c-Casp3
p-Mlkl
Mlkl
g
Scr
ShT2
ShT3
p-NFκB
NFκB
p-Jnk
Jnk
p-Tbk1
Tbk1
p-P38
P38

Figure 3

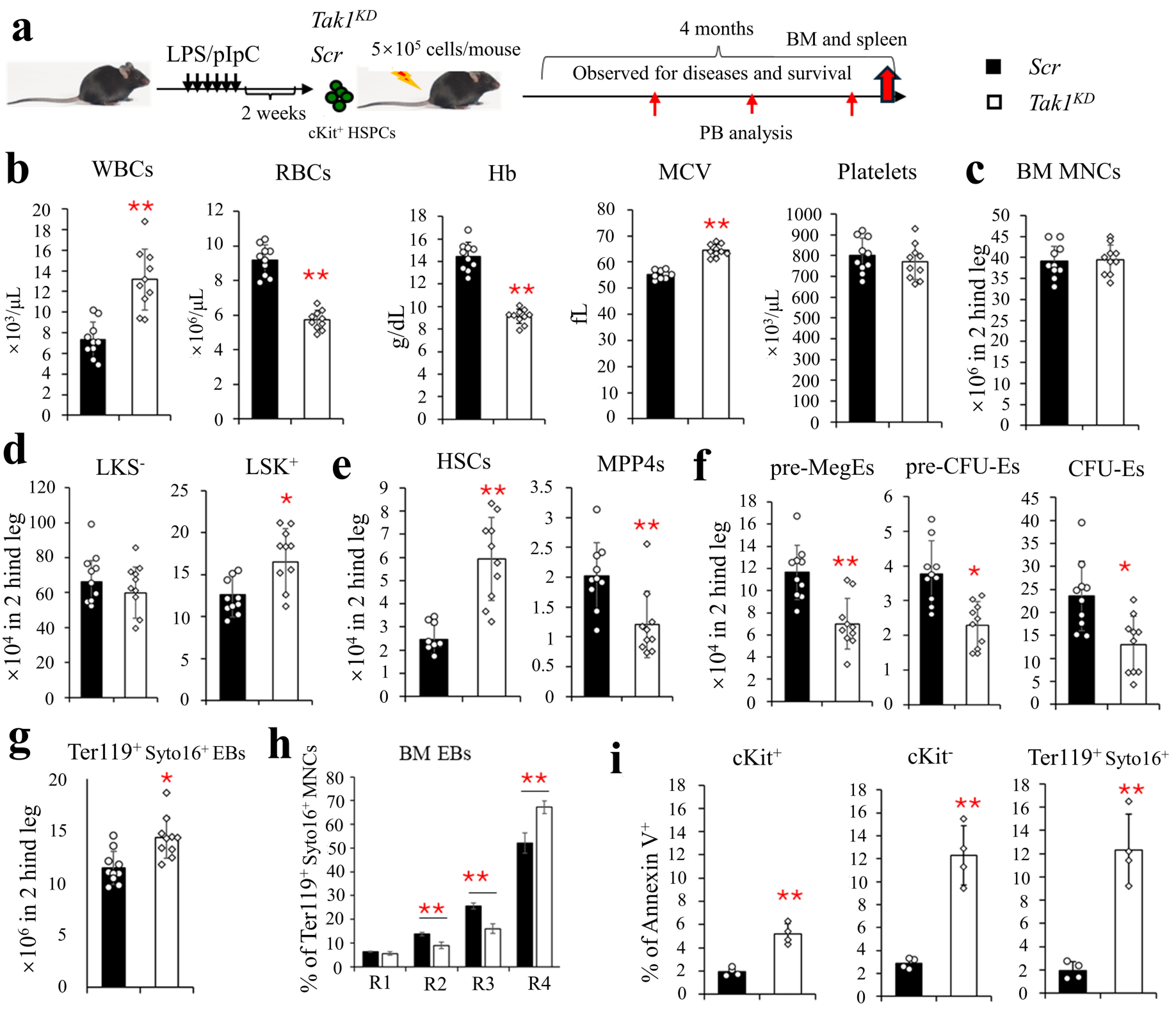
a
Tak1KD
Scr
LPS/pIpC
2 weeks
cKit+ HSPCs
5×10^5 cells/mouse
4 months
BM and spleen
Observed for diseases and survival
PB analysis
Scr
Tak1KD
b
WBCs
RBCs
Hb
MCV
Platelets
×10^3/μL
×10^6/μL
g/dL
fL
×10^3/μL
c
BM MNCs
×10^6 in 2 hind leg
d
LKS-
LSK+
×10^4 in 2 hind leg
e
HSCs
MPP4s
×10^4 in 2 hind leg
f
pre-MegEs
pre-CFU-Es
CFU-Es
×10^4 in 2 hind leg
g
Ter119+ Syto16+ EBs
×10^6 in 2 hind leg
h
BM EBs
% of Ter119+ Syto16+ MNCs
R1
R2
R3
R4
i
cKit+
cKit-
Ter119+ Syto16+
% of Annexin V+

Figure 4

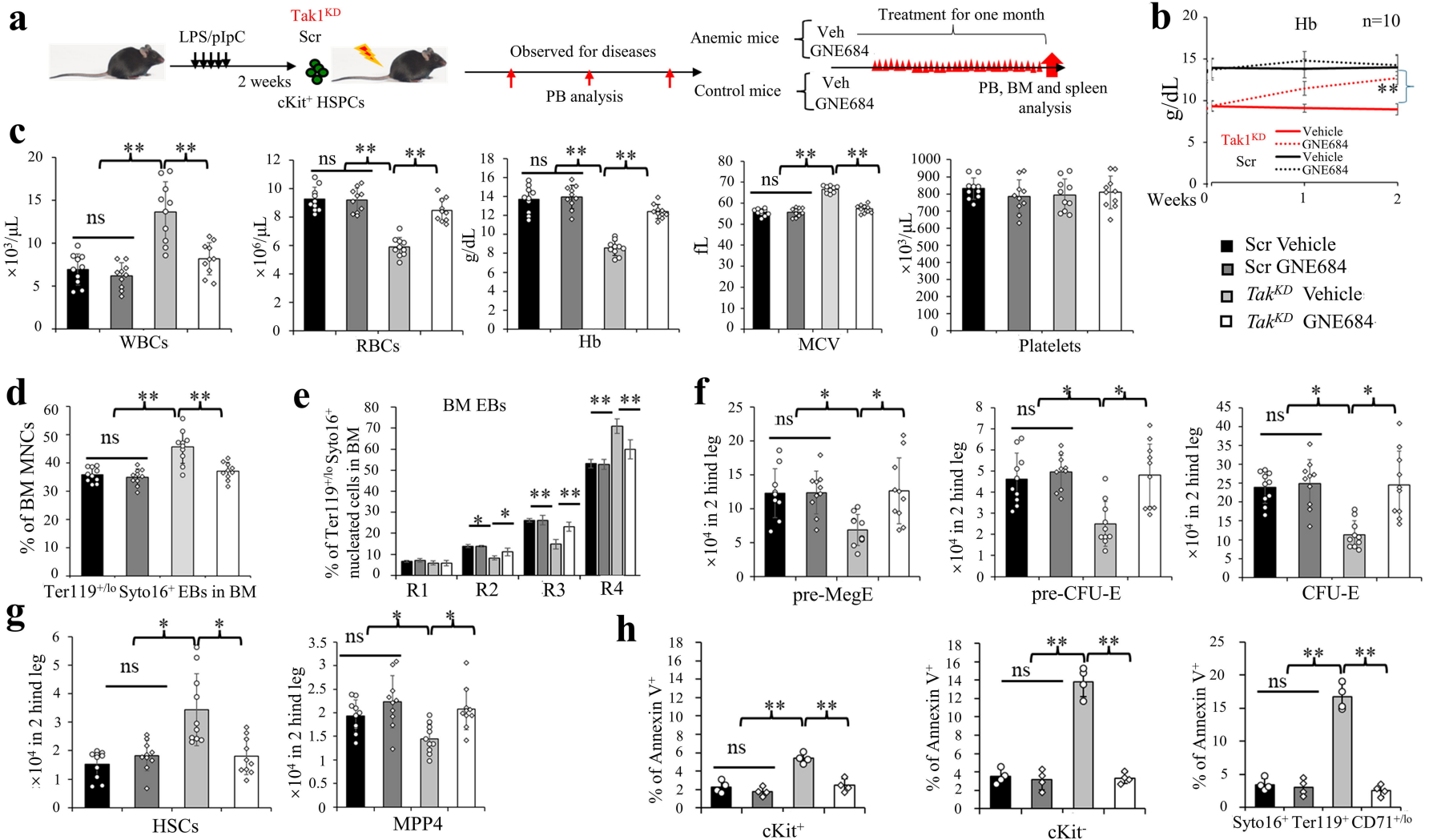
a
LPS/pIpC
Tak1KD
Scr
2 weeks
cKit+ HSPCs
Observed for diseases
PB analysis
Anemic mice
Veh
GNE684
Treatment for one month
Control mice
Veh
GNE684
PB, BM and spleen analysis
b
Hb
n=10
g/dL
Tak1KD
Vehicle
GNE684
Scr
Vehicle
GNE684
Weeks
Scr Vehicle
Scr GNE684
Tak^KD Vehicle
Tak^KD GNE684
c
WBCs
RBCs
Hb
MCV
Platelets
d
% of BM MNCs
Ter119+/lo Syto16+ EBs in BM
e
BM EBs
% of Ter119+/lo Syto16+ nucleated cells in BM
R1
R2
R3
R4
f
pre-MegE
pre-CFU-E
CFU-E
g
HSCs
MPP4
h
% of Annexin V+
cKit+
cKit-
Syto16+ Ter119+ CD71+/lo

Figure 5

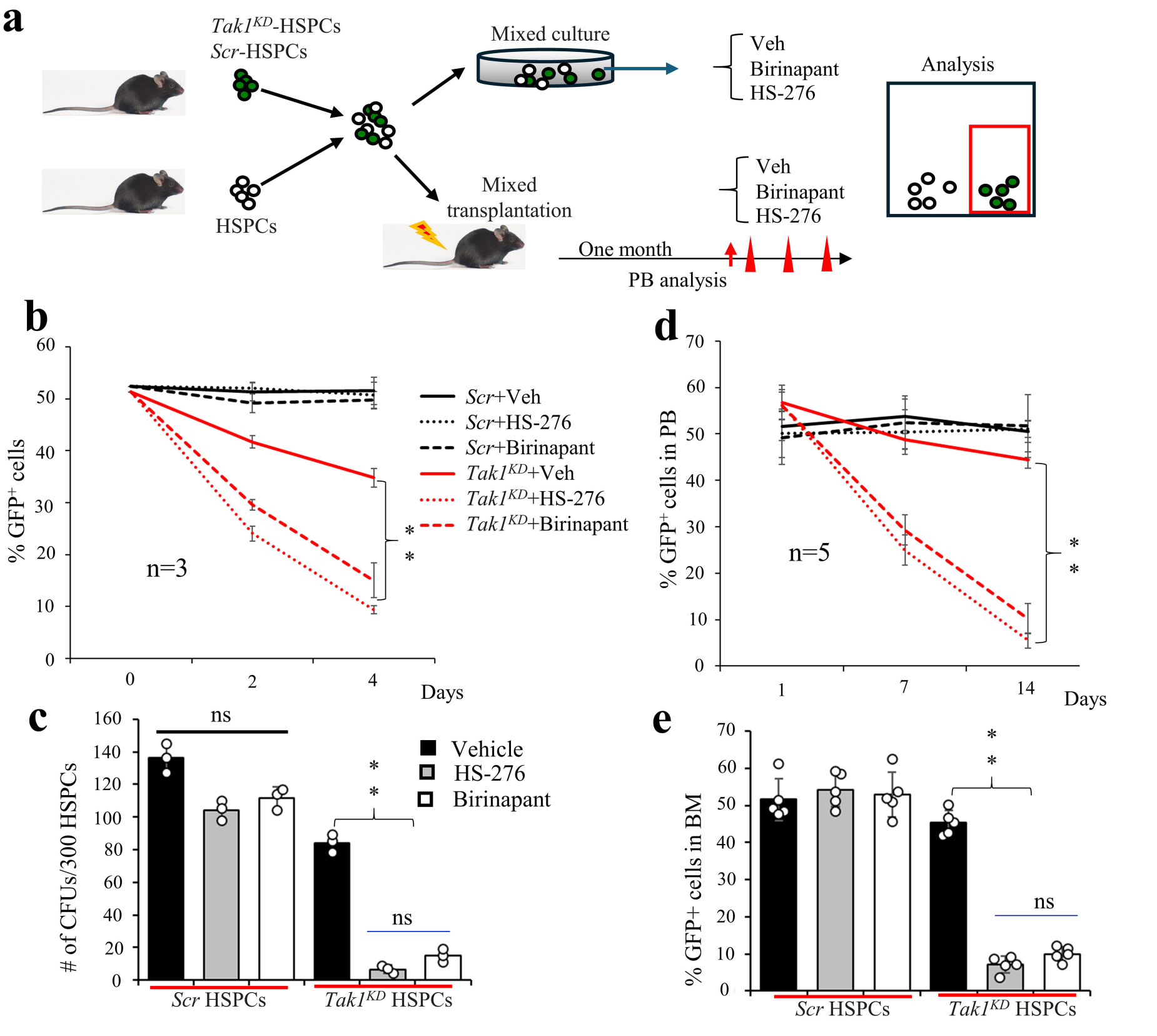
a
Tak1KD-HSPCs
Scr-HSPCs
HSPCs
Mixed culture
Mixed transplantation
Veh
Birinapant
HS-276
Veh
Birinapant
HS-276
Analysis
One month
PB analysis
b
% GFP+ cells
n=3
Days
Scr+Veh
Scr+HS-276
Scr+Birinapant
Tak1KD+Veh
Tak1KD+HS-276
Tak1KD+Birinapant
d
% GFP+ cells in PB
n=5
Days
c
# of CFUs/300 HSPCs
ns
ns
Vehicle
HS-276
Birinapant
Scr HSPCs
Tak1KD HSPCs
e
% GFP+ cells in BM
ns
Scr HSPCs
Tak1KD HSPCs

Figure 6

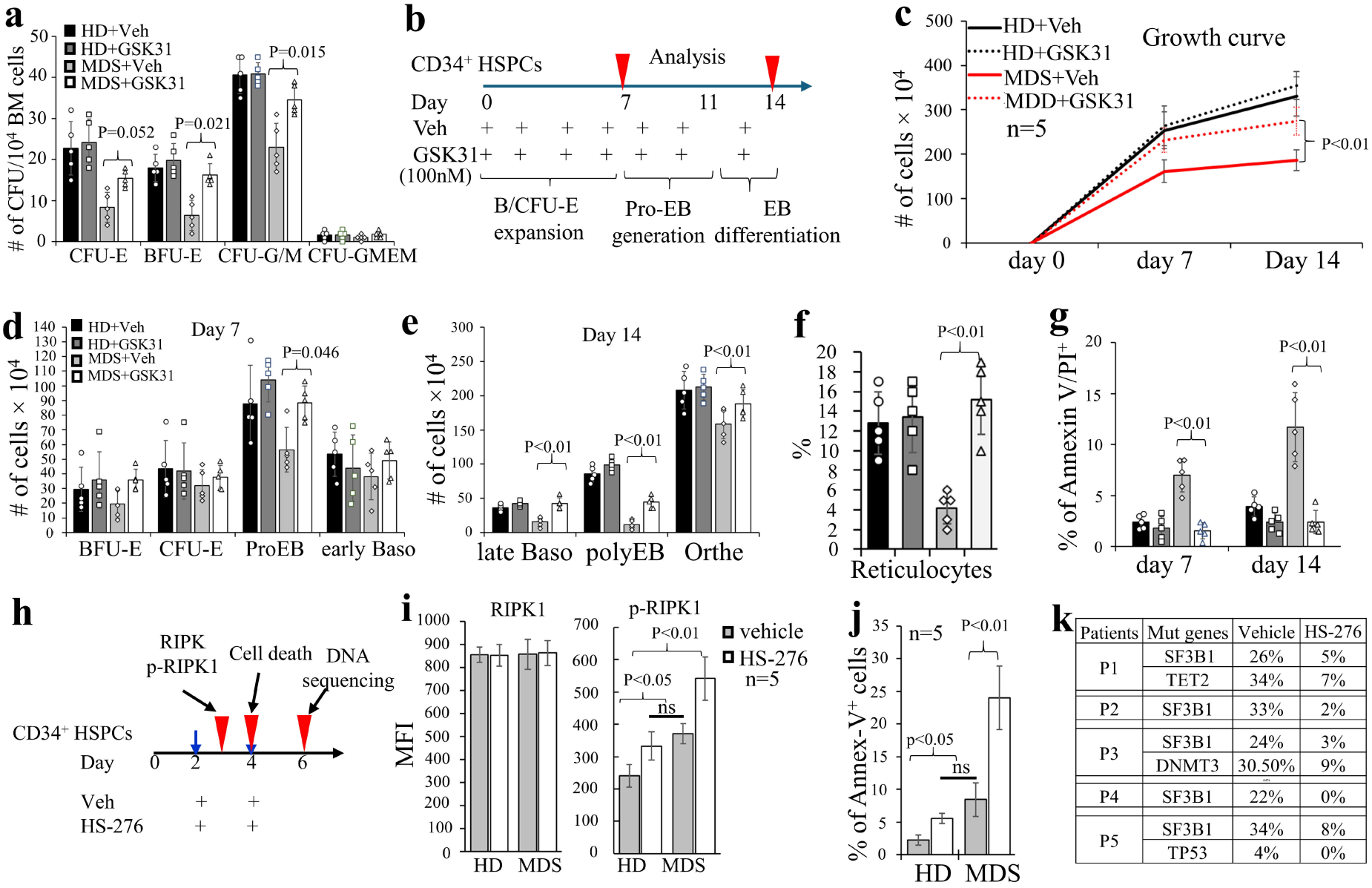

k

Patients	Mut genes	Vehicle	HS-276
P1	SF3B1	26%	5%
	TET2	34%	7%
P2	SF3B1	33%	2%
P3	SF3B1	24%	3%
	DNMT3	30.50%	9%
P4	SF3B1	22%	0%
P5	SF3B1	34%	8%
	TP53	4%	0%

TGFβ-activated kinase-1 knockdown in hematopoietic stem-progenitor cells causes PANoptosis and myelodysplastic syndrome-like disease in mice

Lei Zhang[1,2,3], Wenyan Li[4], Rohit Thalla[2,3], Rongyao Ma[1], Ryan Mack[2,3], Ameet R. Kini[5], Austin Runde[2,3], Patrick A. Hagen[2,6], Kevin Barton[2,6], Jorgena Kosti-Schwartz[2,5], Peter Breslin[2,3,7], Hong-Long Ji[8], Jiwang Zhang[2,3,5*]

[1] Cyrus Tang Hematology Center, Collaborative Innovation Center of Hematology, National Clinical Research Center for Hematologic Diseases, MOE Engineering Center of Hematological Disease, Soochow University, Suzhou 215123, China

[2] Oncology Institute, Cardinal Bernardin Cancer Canter, Loyola University Chicago Medical Center, Maywood, IL 60153, USA

[3] Department of Cancer Biology, Loyola University Chicago Medical Center, Maywood, IL 60153, USA

[4] Lanzhou University Second Hospital, Key Laboratory of Urological Diseases in Gansu Province, Lanzhou, Gansu 730030, China

[5] Departments of Pathology and Radiation Oncology, Loyola University Chicago Medical Center, Maywood, IL 60153, USA

[6]Department of Medicine, Loyola University Chicago Medical Center, Maywood, IL 60153, USA

[7] Departments of Biology and Molecular/Cellular Physiology, Loyola University Chicago, Maywood, IL 60153, USA

[8] Department of Surgery, Loyola University Chicago Medical Center, Maywood, IL 60153, USA

*Corresponding author is Jiwang Zhang, jzhang@luc.edu

Detailed experimental procedures.

Flow cytometric analysis of PANoptosis in patient BM samples. Freshly-isolated or frozen BM cells from MDS patients or healthy donors (HDs) were processed by density gradient centrifugation using Ficoll-Paque™ PLUS to remove debris and dead cells. The mononuclear cells (MNCs) were collected and washed with PBS containing 2% FBS and then fixed and Permeabilized with Cytofix/Cytoperm™ solution (BD Bioscience) on ice for 15 min. according to the manufacturer instructions. After washing with Perm/Wash™ buffer (BD Bioscience), cells were stained with rabbit anti-active CASP3, mouse anti-p-MLKL, or rabbit polyclonal anti-ASC

for 1 h. on ice. After washing with Perm/Wash™ buffer to remove supernatant, cells were incubated on ice for 30 min. with anti-Mouse IgG-Alexa Fluor™ 594 or anti-rabbit-IgG-AlexaFluor488. Cells were then washed again with Perm/Wash™ buffer followed by flow cytometric analysis. Flow data were gated with the FlowJo. For ASC specks, single cells were analyzed by ASC area *vs.* ASC width.[1, 2] Antibodies and reagents used in this experiment are listed in **Tables S2 and S3**.

ShRNA transduction,* in vitro *expansion and transplantation of BM CD117$^+$ HSPCs. Map3k7 Mouse shRNA plasmid (Locus ID 26409) was purchased from Origene. CD117$^+$ HSPCs from *WT* mice and *Rosa26^{CreErt}Casp8$^{fx/fx}$Ripk3$^{-/-}$* mice (30 days after *Casp8* deletion was induced by 5× tamoxifen injections) were isolated by MojoSort™ Mouse CD117 Selection Kit and were cultured (1×10^6/mL) in a serum albumin-free medium for murine HSC expansion at 37°C. in a humidified 5% CO_2 and 5% O_2 incubator. This medium is composed of F12 medium, 1% Insulin-Transferrin-Selenium-Ethanolamine (ITS-X, 100X), 1% Penicillin-Streptomycin-L-Glutamine Solution (P/S/G, 100X), 10mM N-2-hydroxyethylpiperazine-N-2-ethane sulfonic acid (HEPES), 0.1% polyvinyl alcohol (PVA), 100ng/ml mouse TPO and 10ng/ml mouse SCF.[3] After two days of expansion, cells were infected with *sh-Tak1-tGFP*-expressing lentivirus or luciferase shRNA (shLuc)-tGFP-expressing lentivirus by 2 × spinoculation (2,000 × g. for 4 hours at 32°C. each time, with 24 hours between centrifugations) and were incubated in HSC expansion medium for three additional days. The transduced HSPCs were then purified by FACS for GFP$^+$ cells and were further incubated in the HSC expansion medium for 15-16 additional days with medium change every other day. The efficiency of *Tak1* knockdown was verified by RT-PCR and Western blotting. Cells were collected and used for either *in vitro* analysis or *in vivo* transplantation studies.

Transplantation of the transduced HSPCs and in vivo treatments. To study *Tak1^{KD}* in MDS development, the transduced HSPCs that were collected from the above cultures and transplanted into lethally-irradiated (9.5Gy) C57Bl6/J mice by tail-vein injections. Ten recipient mice were used in each group, 5×10^5 cells per recipient. To monitor mice for hematopoietic disease development, PB samples were collected monthly from all recipients and analyzed for WBC counts, platelet counts, RBC counts, Hb concentration and RBC MCV using a Hemavet 950FS (Drew Scientific). Four months post-transplantation, all mice were sacrificed and PB, spleens,

thymuses, and BM were collected for phenotypic analysis by flow cytometry as described previously.[4, 5] All of the fluorescent antibodies used in flow cytometric analyses were purchased from either eBioscience or Biolegend (See **Table S2**). To study the responses of *Tak1*^{KD} MDS to Ripk1 inhibitor treatment *in vivo*, we transplanted another batch of mice. Both male and female mice (1:1 ratio) were used as transplantation recipients. After moderate anemia developed in mice transplanted with *Tak1*^{KD} HSPCs (hemoglobin <10g/l), we randomly divided the mice into two groups with equal distribution of males and females in each group. One group was treated with 50mg/kg GNE684 (a murine Ripk1 inhibitor) twice daily p.o. for 30 days; the mice in the other group were treated with vehicle. Mice transplanted with *scr*-HSPCs were treated and studied in parallel as controls. All mice were euthanized for hematopoietic analysis one day after the last treatment.

To study the responses of *Tak1*^{KD} HSPCs to Tak1 inhibitor and cIAP inhibitor (or Smac-mimetic) treatment *in vivo*, in addition to *Tak1*^{KD} HSPCs and *scr*-HSPCs, we also cultured c-Kit^{+} cells in parallel without infection (non-transduced HSPCs). The *Tak1*^{KD} HSPCs were mixed with non-transduced HSPCs in a 1.5:1 ratio and transplanted into recipient mice. Each mouse received 3×10^5 *Tak1*^{KD} HSPCs and 2×10^5 non-transduced HSPCs. For *scr*-control groups, *scr*-HSPCs were mixed with non-transduced HSPCs in a 1:1 ratio, each mouse receiving 2.5×10^5 *Tak1*^{KD} HSPCs and 2.5×10^5 non-transduced HSPCs. Thirty days after transplantation, the percentages of GFP^{+} cells in PB were examined to determine the contributions of the transduced HSPCs. The mice were then randomly divided into three groups. Mice in groups 1, 2 and 3 were treated with 50mg/kg HS-276, 30mg/kg Birinapant, and vehicle i.p. every other day for 14 days, respectively. Percentages of GFP^{+} cells in PB and BM were examined on the indicated days.

Mouse phenotypic analysis. Peripheral blood was analyzed at indicated time points for WBC counts, plt, RBC counts, and Hb concentration by using Hemavet 950FS (Drew Scientific Inc.). Mice were sacrificed at the indicated time points to collect peripheral blood, spleens, and BM. For HSPC analysis, after lysis of RBCs, MNCs from PB, spleens, and BM were further stained with cell surface markers and analyzed by flow cytometry as described previously[6]. Cells were stained with antibodies directed against CD3ε, B220, Gr1(Ly-6G/Ly-6C), and CD11b to detect mature hematopoietic cell types. For HSC and HPC analysis, 1×10^6 BM MNCs were incubated with BV421-conjugated antibodies against lineage^{+} cells (including CD3ε, B220, Gr-1, CD11b, and

Ter-119), anti-Sca1-PE, anti-cKit-APC, anti-CD48-PECy7, anti-CD150-BV785, anti-CD135-eFluor710, anti-CD105-BV711, anti-CD34-PE-Dazzle594, and anti-CD16/32-PE-Cy7 antibodies. For analysis of murine EBs and reticulocytes from either mouse BM or cultured cells, the cells were pre-incubated with TruStain FcX™ PLUS (anti-mouse CD16/32) antibody (Biolegend, San Diego, CA, USA, cat# 156604) at a concentration of 0.25μg/10^6 cells in a volume of 100μL for 10 min. at a temperature of 2–8°C. to block non-specific binding. The cells were then stained with Ter119 and Syto16 (nuclei) for separating $Ter119^+Syto16^+$ EBs from $Ter119^+Syto16^-$ reticulocytes and mature RBCs[7] (**Figure S3B**). The differentiation stages of EBs were further analyzed by flow cytometry for plotting of CD71 vs. Ter119 with gating the population R1, R2, R3, and R4 for Pro-EBs ($CD71^{hi}Ter119^{lo}$), Baso-EBs ($CD71^{hi}Ter119^{hi}$), Poly-EBs ($CD71^{med}Ter119^{hi}$) and Ortho-EBs ($CD71^-Ter119^{hi}$), respectively (**Figure S3B**).[8, 9] The differentiation stages of EBs were also analyzed by flow cytometry for plotting of CD44 *vs.* FSC with gating the population R1, R2, R3, and R4 for Pro-EBs ($CD44^{hi}FSC^{hi}$), Baso-EBs ($CD44^+FSC^{hi}$), Poly-EBs ($CD44^{med}FSC^{med}$) and Ortho-EBs ($CD44^{lo}FSC^{lo}$), respectively (**Figure S3B**).[8, 9] Because we found that the data from these two EB analysis assays were comparable, we only presented the data from CD71 vs. Ter119 plotting in this paper. We acquired flow cytometric data using a FACS LSR Fortessa cytometer (BD Biosciences) and analyzed them using FlowJo software. Antibodies used in this experiment are listed in **Table S2**.

In vitro erythropoietic culture for murine HSPCs. The basic culture medium for both expansion of murine erythroid progenitors and differentiation of EBs is IMDM containing L-glutamine and 25mM HEPES (Gibco), 20% fetal calf serum (Hyclone), 200μg/ml holotransferrin (Sigma, St. Louis, MO), 10μg/ml recombinant human insulin (Sigma), 1% penicillin/streptomycin (ThermoFisher Scientific) and 10^{-4} M β-Mercaptoethanol (Sigma). For erythroid progenitor expansion, Lin^-Kit^+ BM cells (at a density of 10^5 cells/ml) were cultured in basic medium supplemented with 0.5U/ml Epo (Procrit, Amgen; 1 IU/ml = 1.2ng/ml), 100ng/ml SCF, 10ng/ml IL3 (Peprotech), 10μM dexamethasone (Sigma) and 100ng/ml IGF1 (R&D Systems) with medium change every day for six days. For EB differentiation, cells were collected on day 6 and then were transferred to basic medium supplemented with 0.5U/ml Epo (Amgen) at 5×10^5cells/mL for 3 days with or without Ripk1 inhibitor GNE684 treatment. The cells were collected indicated timepoints for Western blot analysis.

Primary Human Samples. BM biopsies and/or BM aspirates from MDS patients and other hematopoietic diseases were collected at Loyola University Medical Center's clinics (IRB# 205151081313), Hematological Biobank, Jiangsu Biobank of Clinical Resources, and Lanzhou University Secondary Hospital (SUDA20221214H01) after approval of the corresponding Institutional Review Boards and in accordance with the Declaration of Helsinki. The diagnosis of MDS was assigned according to World Health Organization criteria and the risk levels of diseases were stratified using Revised International Prognostic Scoring System (IPSS-R). Baseline BM biopsies and/or aspirates were collected from patients during diagnosis before the initiation of any treatment. Genetic mutations in the patient samples were determined by a targeted amplicon-based next-generation sequencing as a standard clinical procedure. The clinical characteristics of the patients are presented in **Table S4**. BM samples from HDs were obtained from the BM transplantation section at Loyola University Medical Center, USA, and the National Clinical Research Center for Hematologic Diseases in Suzhou, China. Written informed consent was obtained from all donors. For BM biopsies, the tissues were fixed with zinc formalin and processed for paraffin sections. For BM aspirations, cells were first diluted with an equal volume of PBS containing 0.5% BSA and were subsequently separated using the standard gradient separation approach with Ficoll-Paque PLUS (Catalog number #45-001-752, Thermo Fisher Scientific). The MNCs at the interface were collected and washed once at 300 × g. for 10 min. and twice at 200 × g. for 10 min. MNCs were cryopreserved and stored under liquid nitrogen until use. For $CD34^+$ cell enrichment, MNCs were incubated with the CD34 Microbead Kit followed by magnetic-activated cell sorting (MACS) (Catalog number #130-046-702, Miltenyi Biotec). The purity of isolated $CD34^+$ cells (95% to 98%) was verified by flow cytometry.

In vitro erythroid differentiation culture and treatment for human HSPCs. We used the 3-phase erythroid culture system[10] to study MDS erythropoiesis. The basic culture medium for *in vitro* culture of erythroid progenitors is IMDM plus 2% human PB, 3% human AB serum, 200μg/mL Holo-human transferrin, 10μg/mL heparin and 10μg/mL human insulin. In the first phase, $CD34^+$ HSPCs (1×10^5/mL) were incubated in basic medium containing 10ng/mL rhSCF, 1ng/mL rhIL-3 and 1.5IU/mL rhEPO × 6 days with medium change every 2 days to expand BFU-E erythroid progenitors and CFU-E erythroid precursors. In the second phase (days 7-11), IL-3

was removed from the medium to promote the generation of ProE. In the third phase (days 11-15), the cell concentration was adjusted to 10^6/mL on day 11 and cells were cultured in basic medium containing 3IU/mL rhEPO; the concentration of transferrin was adjusted to 1mg/mL to promote the differentiation of EBs.

To study whether RIPK1 inhibition can restore normal differentiation and promote survival of MDS erythroid progenitors, $CD34^+$ HSPCs from MDS patients and HDs were cultured in the 3-phase erythroid culture system as described above and treated with 100nM of the RIPK1 inhibitor GSK3145095 or vehicle. The inhibitor and vehicle were added during medium change every two days. The numbers of phenotypic BFU-E, CFU-E, Pro-EBs, and early-Baso-EBs were analyzed on day 7 of culturing by flow cytometry. The $Syto16^+$ EBs and $Syto16^-$ reticulocytes were analyzed on day 14 of culturing by flow cytometry for Syto16 nuclear staining within the glycophorin A^+ (GPA, $CD235a)^+$ population. The differentiation stages of $Syto16^+$ EBs, including late-Baso-EBs, Poly-EBs and Ortho-EBs, were further analyzed by flow cytometry-based CD105 and CD235a expression. Death of the cultured cells was analyzed on days 7 and 14 by Annexin-V/PI staining. Antibodies and reagents used in this experiment are listed in **Tables S2 and S3**.

In vitro culture and treatment of CD34$^+$ HSPCs. $CD34^+$ HSPCs were incubated in Soluplus-based 3a medium (1% Soluplus + 1μM 740Y-P + 0.1μM butyramide + 70nM UM171) at 37°C. with 5% CO_2 and 10% O_2 for *in vitro* expansion. Medium changes were made every two days by removing half of the medium and replacing it with pre-warmed and freshly-prepared medium.[11] To study the responses of mutant HPSCs to TAK1 inhibitor treatment, HS-276 (10μM final concentration) was added on days 2 and 4 of culturing during medium changes. Cells were collected on day 6 of culturing for targeted DNA-sequencing to detect mutational variant allele frequency (VAF) of the $SF3B1^{mut}$ and other MDS gene mutations.

Colony-forming cell (CFC) assay. BM MNCs from MDS patients and mice were isolated by density-based cell separation using Lymphoprep™. Human cells were seeded in MethoCult® H4434 classic medium at a concentration at 5×10^4/ml (for human) and were incubated at 37°C. in a humidified atmosphere with 5% CO_2. CFU-E colonies were counted on day 7 and BFU-E, CFU-G/M and CFU-GMEM colonies were counted on day 14 by investigators blinded to the experimental conditions. Murine cells were seeded into MethoCult GF M3434 methylcellulose

medium at a concentration of 1×10^4 cells/ml and were incubated at 37°C. in a humidified atmosphere with 5% CO_2. CFU-E colonies were counted on day 3, BFU-E and CFU-G/M were counted on day 7, while CFU-GMEM colonies were counted on day 12 by investigators blinded to the experimental conditions.

Western blotting. Cell lysates from BM MNCs were extracted using Cell Lysis Buffer (Cell Signaling) followed by a brief sonication. The supernatants were collected after centrifugation at 4°C., 14,000 × g. for 20 min. Protein samples were separated by SDS-PAGE on 10% or 12% acrylamide gels. Proteins were transferred onto nitrocellulose membranes to examine the target proteins by antibody blotting. Antibodies used in this study are listed in Antibodies for Western blotting (**Table 3**). The band quantifications using Multi Gauge 3.0 were normalized to corresponding controls, which were set to 1.00 after being normalized to corresponding loading standards on the Western blot.

Real-time RT-PCR analysis. Total RNA was isolated from HSCs and MPP, LSK, and LK cells using TRIzol reagent (Invitrogen, Carlsbad, CA) following the manufacturer's protocol. cDNA was generated from RNA using SuperScript III reverse transcriptase (Life Technologies). The levels of mRNA of the genes of interest were examined by qRT-PCR using the TaqMan assay (Thermo Fisher Scientific) following the instructions provided by the vendor. GAPDH was used as a control. The primers for qRT-PCR used in this study are listed in **Table S1**. The threshold cycle values (CT) for each reaction were determined and averaged using TaqMan SDS analysis software (Applied Biosystems). The changes in target gene expression were calculated by the comparative CT method (fold change = $2[-\Delta\Delta CT]$), as described previously. Each sample was a mixture of LSK HSCs from three mice of the same phenotype. Triplicate RT-PCRs were performed.

Statistical analysis. Data are expressed as the means ± SD. Two-way ANOVA (multiple groups) and Student's t test (two groups) were performed to determine the statistical significance of differences among and between experimental groups. $p < 0.05$ was considered significant. All analyses were done using GraphPad Prism from GraphPad Software (San Diego, CA). The results are presented as means ± standard error (SE) of the mean. An unpaired t-test with Welch correction

was used to determine statistically significant differences between the erythroid cells under normal and hypoxic conditions.

Table S1. Primers

Primer names	Primer sequences	Product sizes
TAK1 f1	5'-GGCTTTCATTGTGGAGGTAAGCTGAGA-3'	320bp for floxed allele
TAK1 r1	5'-GGAACCCGTGGATAAGTGCACTTGAAT-3'	280bp for WT allele
TAK1 f2	5'-GCAACTTCGACAACTTGCCTTCCTGTG-3'	
TAK1 r2	5'-GCACTTGAATTAGCGGCCGCAAGCTTATAACT-3'	1000bp for mutant allele
Cre1	5'-CTAGGCCACAGAATTGAAAGATCT-3'	
Cre2	5'-GTAGGTGGAAATTCTAGCATCATC C-3'	324 bp for Cre
Cre3	5'-GCGGTCTGGCAGTAAAAACTATC-3'	
Cre4	5'-GTGAAACAGCATTGCTGTCACTT-3'	100 bp for internal control
Map3k7	Mm01191861_m1	ThermoFisher Scientific Catalog # 4351372
Gapdh	Mm99999915_g1	ThermoFisher Scientific Catalog # 4331182

Table S2. List of antibodies used in this study

Antibodies	**Venders**	**Catalogue #**
Antibodies for analysis of murine HSCs and HPCs		
Brilliant Violet 421™ anti-mouse Ly-6G/Ly-6C (Gr-1) Antibody	Biolegend	108434
Brilliant Violet 421™ anti-mouse CD3ε Antibody	Biolegend	100336
Brilliant Violet 421™ anti-mouse B220 Antibody	Biolegend	103240
Brilliant Violet 421™ anti-mouse TER-119/Erythroid Cells Antibody	Biolegend	116233
PE anti-mouse Ly-6A/E (Sca-1) Antibody	Biolegend	108108
BV605-anti-mouse Ly-6A/E (Sca1)	BioLegend	108134
APC anti-mouse CD117 (c-Kit) Antibody	Biolegend	105812
APC/Cy7 anti-mouse CD48 Antibody	Biolegend	103431
PE/Cy7 anti-mouse CD150 (SLAM) Antibody	Biolegend	115914
PE/Cyanine5 anti-mouse CD105 Antibody	Biolegend	120428
APC/Cyanine7 anti-mouse CD105 Antibody	Biolegend	120432
PE/Cy5 anti-mouse CD135 Antibody	Biolegend	135312
PerCP/Cy5.5 anti-mouse CD127 (IL-7Rα) Antibody	Biolegend	135022
CD41a Monoclonal Antibody (eBioMWReg30 (MWReg30)), PerCP-eFluor 710	Life technologies	46-0411
PE/Cyanine7 anti-mouse CD41	BioLegend	133915
PE/Cyanine7 anti-mouse CD16/32	BioLegend	101318
BV510 anti-mouse CD16/32	BioLegend	101333
PE/Dazzle594 anti-mouse CD34	BioLegend	128616
PE-Cy7 anti-mouse CD3e	BD Bioscience	552774
PE anti-mouse CD11b	Thermo Fisher Scientific	12-0112-85
APC Anti-human/mouse CD45R	Thermo Fisher Scientific	17-0452-82
PE anti-mouse CD8a	Thermo Fisher Scientific	12-0081-82
APC Anti-mouse CD4	Thermo Fisher Scientific	17-0041- 83
FITC CD3e Monoclonal Antibody (145-2C11),	Thermo Fisher Scientific	11-0031-82
Pacific Blue™ anti-mouse TER-119	Biolegend	116232
BV510 anti-mouse TER119	BioLegend	116237
PE anti-mouse/human CD44 Antibody	BioLegend	103024
Anti-mouse CD44-BV650	BioLegend	103049
APC anti-mouse CD71 Antibody	BioLegend	113820
syto-16	ThermoFisher Scientific	S7578
Anti-human antibodies for HSC and erythroblast analysis		
PE/Cyanine7 anti-human CD123 Antibody	BioLegend	306010
Brilliant Violet 421™ anti-human CD235a (Glycophorin A) Antibody	BioLegend	349132
PE anti-human CD235a (Glycophorin A) Antibody	BioLegend	349106
APC anti-human CD34 Antibody	BioLegend	378606
BD Horizon™ V450 Mouse Anti-Human CD38	BD Biosciences	561378

APC anti-human CD41	BioLegend	984504
Brilliant Violet 510™ anti-human CD41 Antibody	BioLegend	303736
Alexa Fluor® 700 anti-human CD45RA Antibody	BioLegend	304120
APC/Cyanine7 anti-human CD71 Antibody	BioLegend	334110
BD Horizon™ PE-CF594 Mouse Anti-Human CD105	BD Biosciences	562380
APC anti-human CD105 Antibody	BioLegend	323208
PerCp-conjugated anti-CD3, anti-CD4, anti-CD14, and anti-CD19		
Antibodies for Western Blotting		
TAK1 (D94D7) Rabbit mAb (human and mouse)	Cell Signaling Technology	5206
RIP (D94C12) XP® Rabbit mAb (human and mouse)	Cell Signaling Technology	3493
Phospho-RIP (Ser166) (D8I3A) Rabbit mAb (human and mouse)	Cell Signaling Technology	96323
Gasdermin D (E9S1X) Rabbit mAb (human and mouse)	Cell Signaling Technology	39754
Caspase-8 (D35G2) Rabbit mAb (human and mouse)	Cell Signaling Technology	4790
Cleaved Caspase-1 (Asp296) (E2G2I) Rabbit mAb (mouse)	Cell Signaling Technology	89332
Cleaved Caspase-1 (Asp297) (D57A2) Rabbit mAb (human)	Cell Signaling Technology	4199
β-Actin (13E5) Rabbit mAb (human and mouse)	Cell Signaling Technology	4970
NF-κB p65 (D14E12) XP® Rabbit mAb (human and mouse)	Cell Signaling Technology	8242
Phospho-NF-κB p65 (Ser536) (93H1) Rabbit mAb (human and mouse)	Cell Signaling Technology	#3033
TBK1/NAK (D1B4) Rabbit mAb (human and mouse)	Cell Signaling Technology	#3504
Phospho-TBK1/NAK (Ser172) (D52C2) XP® Rabbit (human and mouse)mAb	Cell Signaling Technology	#5483
p38 MAPK (D13E1) XP® Rabbit mAb (human and mouse)	Cell Signaling Technology	#8690
Phospho-p38 MAPK (Thr180/Tyr182) (D3F9) XP® Rabbit mAb (human and mouse)	Cell Signaling Technology	#4511
SAPK/JNK Antibody (human and mouse)	Cell Signaling Technology	#9252
Phospho-SAPK/JNK (Thr183/Tyr185) (81E11) Rabbit mAb (human and mouse)	Cell Signaling Technology	#4668
Phospho-MLKL (Ser358) Polyclonal Antibody (human)	ThermoFisher Scientific	PA5-105678
Phospho-MLKL (Ser358) (D6H3V) Rabbit mAb #91689 (human)	Cell Signaling Technology	91689
Phospho-MLKL (Ser345) (D6E3G) Rabbit mAb (BSA and Azide Free) (mouse)	Cell Signaling Technology	17825
MLKL (E7V4W) Mouse mAb (BSA and Azide Free) (both human and mouse)	Cell Signaling Technology	44621
Antibodies for intracellular staining and immunofluorescence staining		
Cleaved Caspase-3 (Asp175) Antibody (Rabbit)	Cell Signaling Technology	9661
Human Phospho-MLKL (T357) Antibody (mouse) Phospho-MLKL (Ser358) Polyclonal Antibody (Rabbit)	R&D system ThermoFisher Scientific	MAB9187-100 PA5-105678
Anti-ASC Antibody, clone 2EI-7 (mouse)	Millipore Sigma	04-147
Goat anti-Mouse IgG (H+L) Cross-Adsorbed Secondary Antibody, Alexa Fluor™ 488	ThermoFisher Scientific	A-11001
Goat anti-Mouse IgG (H+L) Cross-Adsorbed Secondary Antibody, Alexa Fluor™ 594	ThermoFisher Scientific	A-11005
Goat anti-Rabbit IgG (H+L) Cross-Adsorbed Secondary Antibody, Alexa Fluor™ 488	ThermoFisher Scientific	A-11008
Goat anti-Rabbit IgG (H+L) Cross-Adsorbed Secondary Antibody, Alexa Fluor™ 594	ThermoFisher Scientific	A-11012
Goat anti-Rat IgG (H+L) Cross-Adsorbed Secondary Antibody, Alexa Fluor™ 647	ThermoFisher Scientific	A-21247
Goat anti-Rabbit IgG (H+L) Cross-Adsorbed Secondary Antibody, Alexa Fluor™ 568	ThermoFisher Scientific	A-11011

Table S3. Chemical reagents

Chemicals	Venders	Catalog No.
Small molecular inhibitors		
Birinapant (xIAP inhibitor or Smac mimetic)	Medchemexpress	HY-16591
GNE684 (murine RIPK1 inhibitor)	Medchemexpress	HY-128585
GSK3145095 (Human RIPK1 inhibitor)	Medchemexpress	HY-111946
HS-276 (TAK1 inhibitor)	Medchemexpress	HY-147141E1155
Necrostatin 1S (Nec-1S)	Medchemexpress	HY-14622A
VX-765 (Belnacasan) Caspase-1/4 inhibitor	Selleckchem	No.S2228
Z-VAD-FMK (Pan-caspase)	Selleckchem	No.S7023
Z-IETD-FMK (Caspase-8)	Selleckchem	S7314
CA-074 Me (cathepsin B)	Medchemexpress	HY-103350
Cell culture reagents		
Luciferase shRNA (shLuc)-tGFP lentiviral plasmid	Origene	TR30023
Map3k7 Mouse shRNA Plasmid (Locus ID 26409)	Origene	TL516837
1× Ham's F-12 Nutrient Mix liquid media	Life Technologies (Gibco)	
Insulin-Transferrin-Selenium-Ethanolamine (ITS-X, 100X)	Thermo Fisher Scientific	51500-056
Penicillin-Streptomycin-L-Glutamine Solution (P/S/G, 100X)	Thermo Fisher Scientific	10378016
N-2-hydroxyethylpiperazine-N-2-ethane sulfonic acid (HEPES)	Thermo Fisher Scientific Gibco	
Polyvinyl alcohol (PVA)	Sigma	P8136
Mouse TPO (Thrombopoietin) Recombinant Protein, PeproTech® (rmTPO)	Thermo Fisher Scientific Gibco	315-14
Mouse SCF Recombinant Protein, PeproTech® (rmSCF)	Thermo Fisher ScientificGibco	250-03
IMDM (Iscove's Modified Dulbecco's Medium)	Life Technologies (Gibco)	12440-053
100× Insulin-Transferrin-Selenium-ethanolamine (ITS-X)	Life Technologies (Gibco)	51500-056
100× Penicillin-Streptomycin-Glutamine (P/S/G)		10378-016

740Y-P	InvivoChem	V2540
Butyzamide	InvivoChem	V51526
UM171	InvivoChem	V1894
PCL-PVAc-PEG (Soluplus®)	BASF Pharma	402932-23-4
Human PB plasma	Stem Cell Technologies	70039.3
Human AB serum	Sigma-Aldrich	H4522
Holo-human transferrin	Sigma-Aldrich	T4132
heparin	Stem Cell Technologies	7980
human insulin	Sigma-Aldrich	I9278
rhSCF	PeproTech	300-07
rhIL-3	PeproTech	200-03
rhEPO	PeproTech	100-64
MojoSort™ Mouse CD117 (c-Kit) Selection Kit	Biolegend	480146
MethoCult® GF H4434 classic medium	Stem Cell Technologies, Vancouver, BC	04434
MethoCult® GF M3434 medium	Stem Cell Technologies, Vancouver, BC	03434
Reagents for immunofluorescence staining		
Citrate Buffer (pH 6.0), Concentrate	ThermoFisher Scientific	005000
eBioscience™ IHC Antigen Retrieval Solution - Low pH (10X)	ThermoFisher Scientific	00-4955-58
eBioscience™ IHC Antigen Retrieval Solution - High pH (10X)	ThermoFisher Scientific	00-4956-58
Universal antigen retrieval buffer	BiCell Scientific	BCASUB
SlowFade™ Diamond Antifade Mountant with DAPI	ThermoFisher Scientific	S36964
10X Blocking Buffer	abcom	ab126587

Table S4. Patient and control samples used for flow cytometry, immunofluorescent staining, and Western Blotting analysis of PANoptosis

Patients	Gender	Age (Y)	Mutant genes (VAF)	Pathologic Diagnosis	Experiments
P1	Male	57	*SF3B1* (42%) *TET2* (41%)	MDS-RS-MLD	Flow cytometry
P2	Male	71	*SF3B1* (40%)	MDS-RS-SLD	Flow cytometry
P3	Female	64	*SF3B1* (36%) *DNMT3A* (39%)	MDS-RS-MLD	Flow cytometry
P4	Male	72	*SF3B1* (33%)	MDS-RS-SLD	Flow cytometry
P5	Female	58	*SF3B1* (35%) *TP53* (6%)	MDS-RS-MLD	Flow cytometry
P6	Male	66	*SF3B1* (28%) ASXL1 (16%)	MDS-RS-MLD	Flow cytometry
P7	Male	75	*SF3B1* (38%)	MDS-RS-SLD	Flow cytometry
P8	Female	61	*SF3B1* (35%) *TET2* (37%)	MDS-EB1	Flow cytometry
P9	Female	55	*SF3B1* (31%) *STAG2* (11%)	MDS-EB1	Flow cytometry
P10	Male	71	*SF3B1* (39%)	MDS-RS-SLD	Flow cytometry
P11	Male	69	*SF3B1* (33%) *JAK2* (14%)	MDS-RS-MLD	Flow cytometry
P12	Male	75	*SF3B1* (44%) *TET2* (24%)	MDS-RS-MLD	Flow cytometry
P13	Male	78	*SF3B1* (37%)	MDS-RS-SLD	Flow cytometry
P14	Female	69	*SF3B1* (34%) ASXL1 (13%)	MDS-RS-MLD	Flow cytometry
P15	Female	59	*SF3B1* (36%) *BCOR* (11%)	MDS-RS-MLD	Flow cytometry
P16	Female	72	*SRSF2* (24%) *TET2* (31%) *CBL* (5%)	MDS-EB1	Flow cytometry
P17	Male	67	*SRSF2* (27%) *TET2* (31%)	MDS-MLD	Flow cytometry
P18	Female	65	*SRSF2* (23%) *TET2* (34%) *ASXL1* (15%)	MDS-EB2	Flow cytometry
P19	Female	65	*SRSF2* (35%) *NRAS* (6%)	MDS-MLD	Flow cytometry
P20	Male	54	*SRSF2* (32%) *ASXL1* (14%)	MDS-MLD	Flow cytometry
P21	Male	67	*SRSF2* (26%) *EZH2* (17%)	MDS-EB1	Flow cytometry
P22	Female	70	*TET2* (24%)	MDS-MLD	Flow cytometry
P23	Male	62	*TET2* (31%) *DNMT3A* (18%)	MDS-MLD	Flow cytometry
P24	Male	71	*TET2* (34%) *ASXL1*(15%)	MDS-MLD	Flow cytometry
P25	Female	60	*DNMT3A* (21%) *TP53* (13%)	MDS-EB1	Flow cytometry
P26	Male	71	*SF3B1* (35%) *ASXL1* (12%)	MDS-RS-MLD	IF staining *
P27	Male	68	*SF3B1* (21%) *DNMT3A* (31%)	MDS-RS-SLD	IF staining
P28	Female	59	*SSF3B1* (39%)	MDS-RS-SLD	IF staining
P29	Male	72	*SF3B1* (33%)	MDS-RS-SLD	IF staining
P30	Female	66	*SF3B1 (25%) TET2* (34%)	MDS-RS-MLD	IF staining
P31	Male	73	*SSF3B1* (41%)	MDS-RS-SLD	Western Blotting
P32	Male	64	*SF3B1* (38%)	MDS-RS-SLD	Western Blotting
P33	Female	71	*SF3B1 (35%) BCOR* (21%)	MDS-RS-MLD	Western Blotting
C1	Female	63		ID anemia [&]	Flow cytometry
C2	Female	57		ID anemia	Flow cytometry
C3	Male	68		FAD anemia [#]	Flow cytometry
C4	Female	62		ID anemia	Flow cytometry
C5	Male	69		FAD anemia	Flow cytometry

C6	Male	65		FAD anemia	IF staining
C7	Female	57		ID anemia	IF staining
C8	Female	72		FAD anemia	IF staining
C9	Female	73		ID anemia	IF staining
C10	Male	65		FAD anemia	IF staining
C11	Male	56		ID anemia	Western Blotting
C12	Female	61		FAD anemia	Western Blotting
C13	Female	55		FAD anemia	Western Blotting

*Immunofluorescence staining: IF; #Folic acid deficiency anemia: FAD anemia; &Iron-deficiency anemia: ID anemia.

Table S5. Patient and control samples used for *in vitro* culture study

Patients	Gender	Age (Y)	Mutant genes (VAF)	Pathologic Diagnosis
P34	Male	63	*SF3B1* (26%) *TET2* (34%)	MDS-RS-MLD
P35	Male	68	*SF3B1* (33%)	MDS-RS-SLD
P36	Male	66	*SF3B1* (24%) *DNMT3A* (30.5%)	MDS-RS-SLD
P37	Female	59	*SF3B1* (22%)	MDS-RS-SLD
P38	Male	68	*SF3B1* (34%) *TP53* (4%)	MDS-RS-MLD
C14	Male	61		FAD anemia
C15	Female	53		FAD anemia
C16	Female	65		ID anemia
C17	Mail	48		ID anemia
C18	Female	46		FAD anemia

Supplementary data.

Figure S1. Down-regulation of TAK1 protein in CD34$^+$ HSPCs from BM of *SF3B1^{mut}* MDS patients (associated with Figure 1). CD34$^+$ HSPCs were enriched from BM of 2 *SF3B1^{mut}* MDS patients and 2 age-matched healthy donors (HD). TAK1 protein was examined by Western blotting.

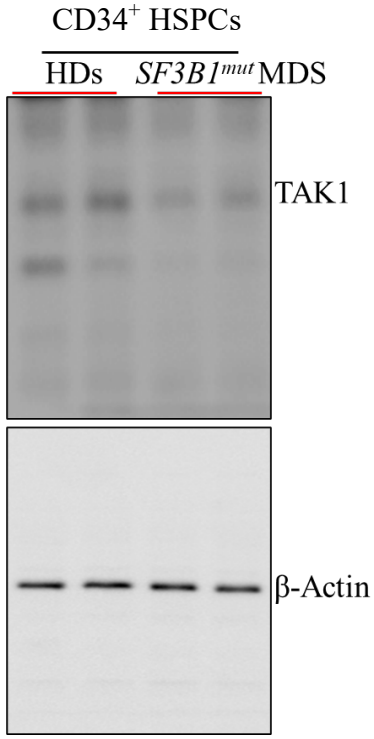

Figure S2. *Tak1*$^{-/-}$ induces PANoptosis and lysosome death in HSPCs (associated with Figure 2). c-Kit^{+} HSPCs from *Tak1*$^{fx/fx}$ *HSPCs* and *Tak1*$^{fx/fx}$*Casp8*$^{-/-}$*Ripk3*$^{-/-}$ mice were transduced with *Cre-GFP or vector-GFP*. One day post-transduction, after determining the transduction efficiency (GFP^{+} cells %), cells were treated with 20μM of pan-Casp inhibitor (Z-VAD) or 20μM of cathepsin B inhibitor (CA-074Me) daily. The relative rate of PCD of the *Tak1*^{KD} HSPCs was evaluated by detecting the GFP^{+}% every 2 days. Vehicle treatments (veh) were studied in parallel as controls. Triplicate experiments were conducted. ** indicates $p<0.01$.

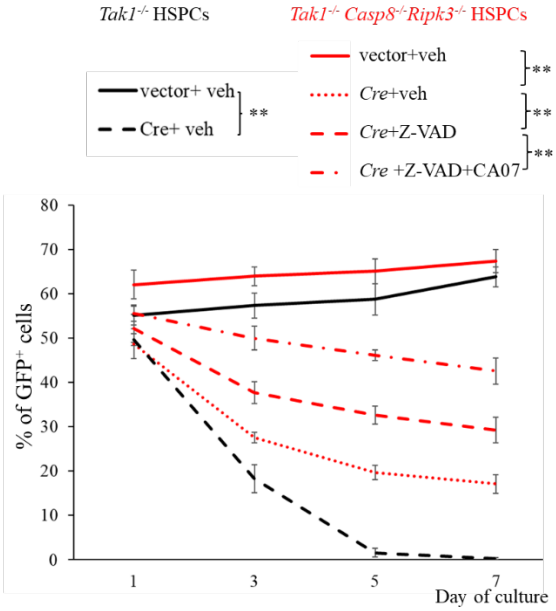

Figure S3. Gating strategies for flow cytometric analysis of HSPCs and EBs (associated with Figure 2-4). a-b. Gating strategy for flow cytometric analysis of BM HSPCs[12] (**a**) and EBs (**b**). HSCs: hematopoietic stem cells; MPP: multipotent progenitor; pre-GM: pre-granulocyte-macrophage progenitor; MkP: megakaryocytic progenitor; GMP: granulocyte-monocyte progenitor; CFU-E: colony forming unit-erythroid; EB: erythroblast; Ret: reticulocyte; RBC: red blood cells; R1: proerythroblast; R2: basophilic erythroblast; R3: polychromatophilic erythroblast, and R4: orthochromatic erythroblast. Syto16 and Ter119 staining was used to separate EBs from RBCs.[7] Two assays were used in analyzing differentiation stages of EBs in **b**.[8, 9] We found the data from two assays were comparable.

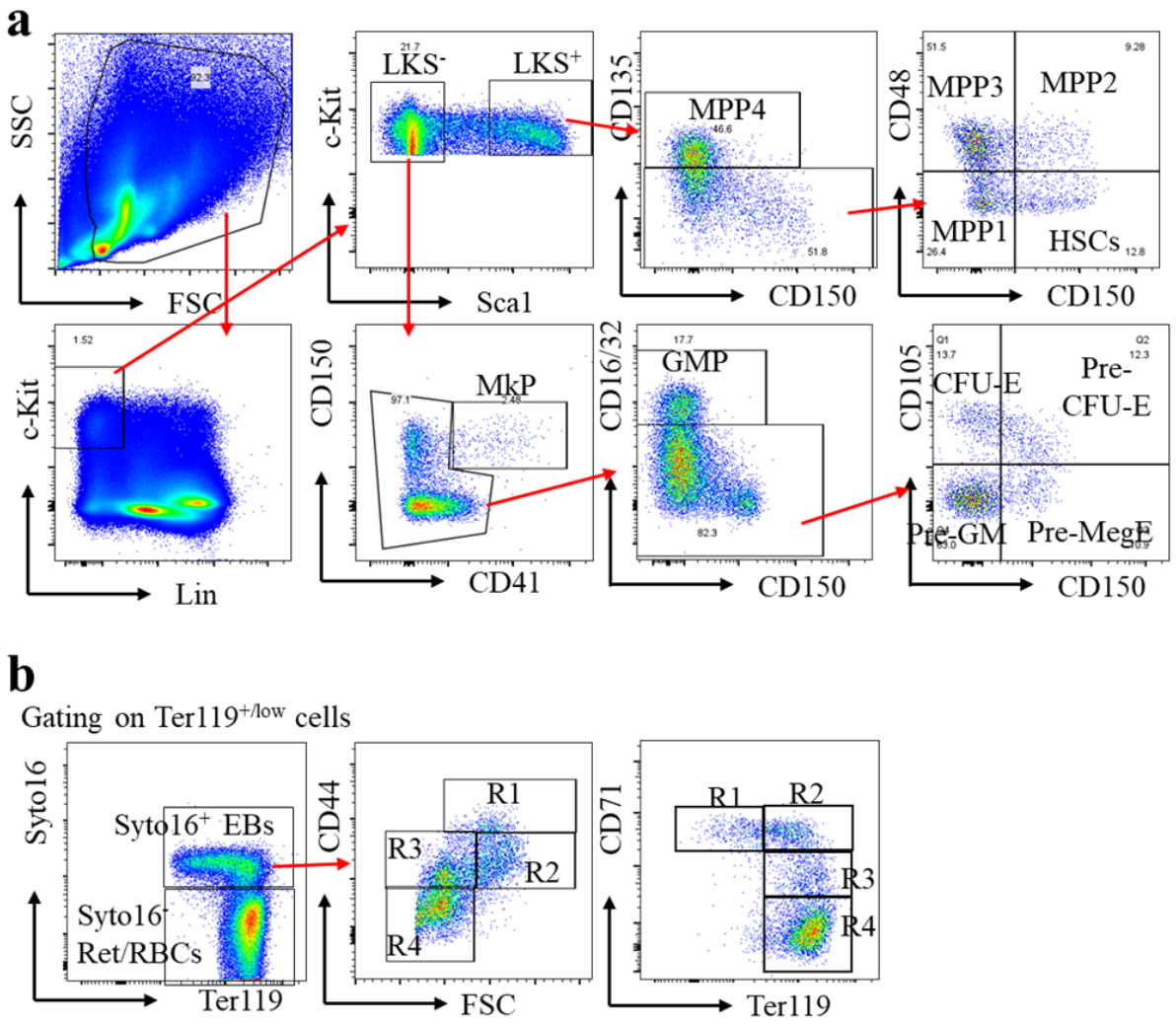

Figure S4. ***Tak1*^{KD} induces PANoptosis in HSPCs without lysosome death (associated with Figure 2).** **a**. c-Kit$^+$ HSPCs from *WT* mice were transduced with 3 shRNA for *Tak1*, respectively. Cells were collected on day two of transduction and PCD was examined by flow cytometry for Annexin V/PI staining as well as ASC speck, pMlkl and a-Casp3 staining. Scrambled shRNA (Scr) transduction was studied in parallel as a control. Triplicate experiments were conducted. ** indicates p<0.01. ns stands for not significant. **b**. c-Kit$^+$ HSPCs from *WT* and *Casp8*$^{-/-}$*Ripk3*$^{-/-}$ mice were transduced with *sh3Tak1* or *Scr*. One day post-transduction, after determining the transduction efficiency (GFP$^+$ cells %), cells were treated with 20μM pan-Casp inhibitor (Z-VAD) or 20μM Ripk1 inhibitor (Nec1s) daily. The relative rate of PCD of the *Tak1*^{KD} HSPCs was evaluated by detecting GFP$^+$% every 2 days. Vehicle treatments (veh) were studied in parallel as controls. Triplicate experiments were conducted. ** indicates p<0.01. **c**. c-Kit$^+$ HSPCs from *Casp8*$^{-/-}$*Ripk3*$^{-/-}$ mice were transduced with *sh2Tak1, sh3Tak1* or *Scr*. One day post-transduction, after determining the transduction efficiency (GFP$^+$ cells %), cells were treated with 20μM Z-VAD, 20μM Z-VAD + 20μM cathepsin B inhibitor CA-074Me, or 20μM CASP1/4 inhibitor VX-765. Triplicate experiments were conducted. ns indicates no-significance.

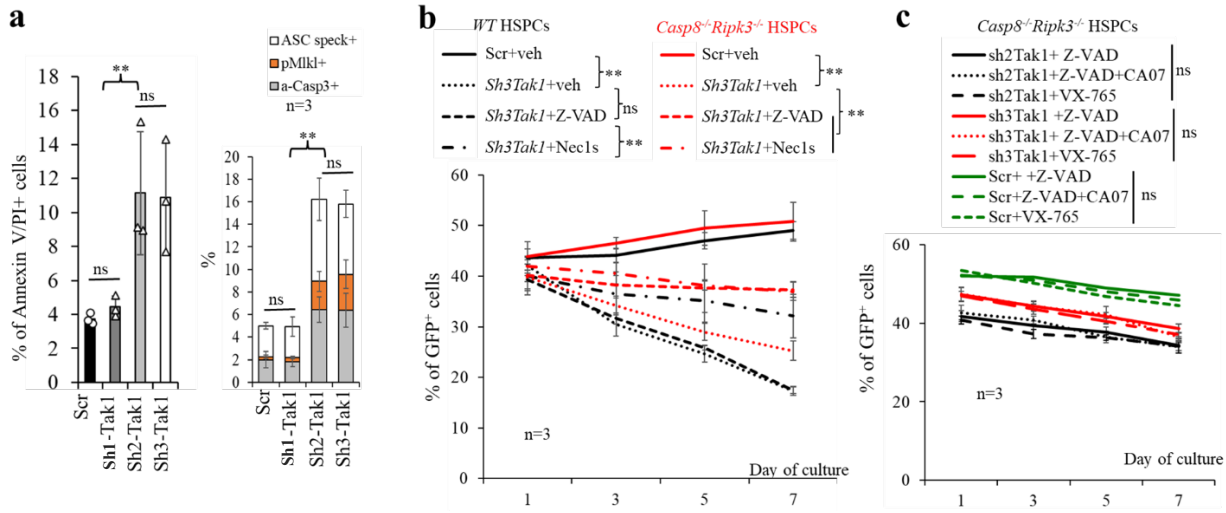

Figure S5. Mice transplanted with *Tak1*^{KD} HSPCs developed MDS-like diseases (associated with Figure 3). **a**. c-Kit$^+$ HSPCs were transduced with *Scr* or *sh3Tak1* and then expanded in HSC expansion medium for 16 days[3]. The phenotype of expanded HSCs was analyzed by flow cytometry. **b-e**. Four months post-transplantation of *Scr*-HSPCs and *Tak1*^{KD} HSPCs, PB and BM were collected from the recipient mice and analyzed by flow cytometry for neutrophils, monocytes and CD3$^+$/B220$^+$ lymphocytes in PB (**b**), GFP$^+$ cell% in PB WBCs and BM MNCs (**c**) as well as for GFP$^+$ cell% in BM Lin$^-$c-Kit$^+$ HSPCs (**d**), as well as the numbers of MPP1, MPP2, MPP3, Pre-GM, GMP and MkP in BM (**e**).

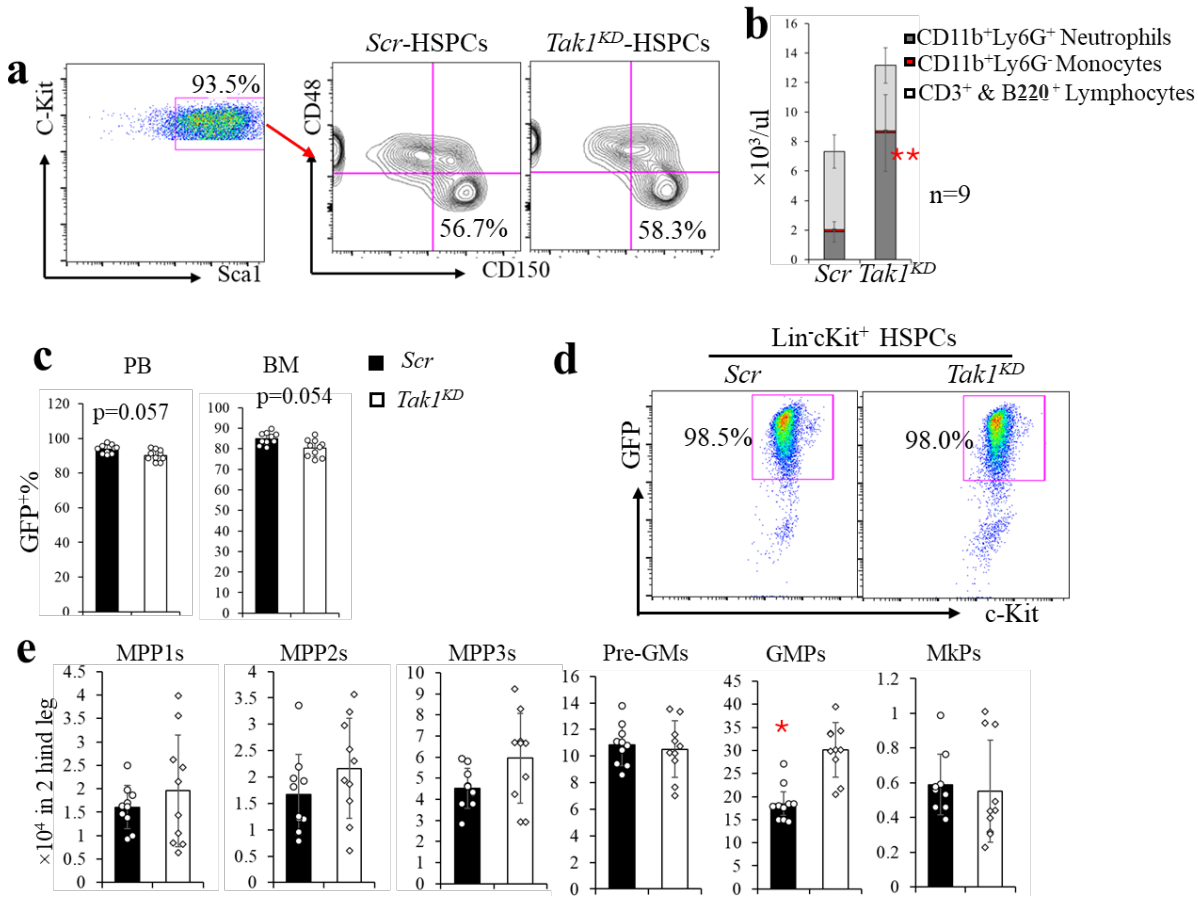

Figure S6. Ripk1 inhibition restores normal BM hematopoiesis and blood cell counts to anemic *Tak1*^{KD} mice (associated with Figure 4). a-d. After anemia developed (Hb<10g/dl) in mice transplanted with *Tak1*^{KD} HSPCs, the mice were randomly separated into two groups and treated with vehicle or GNE684, respectively, for one month. scr-HSPC transplantations were treated and studied in parallel as controls. PB WBC counts, RBC counts and MCV were analyzed on one day before the treatment (0) as well as at 1 and 2 weeks during the treatment (**a**). One day after the last treatment, mice were sacrificed for hematopoietic analysis. GFP^{+} cell% in PB WBCs and BM MNCs (**b**), as well as the number of MNCs (**c**) and MPP4 (**d**) in BM were analyzed by flow cytometry. * Indicates p<0.05. ns indicates no significance. **e-g**. *Tak1*^{KD} and *scr*-HSPCs were cultured in a two-phase *in vitro* erythropoiesis system. After 6 days of growth in expansion medium, the cells were transferred into differentiation medium for further incubation without (**e and f**) or with 30μM Nec1s, or 20μM ZIETD (CASP8 inhibitor)/GSK-872 (RIPK3 inhibitor) treatment (**g**). Cells were collected at 12, 24 and 48 hours of culturing for Gata1 protein levels by Western blotting (**e** and **g**), or at 24 hours of culturing for EB analysis by flow cytometry (**f**). **h**. *Tak1*^{KD} and *scr*-HSPCs were cultured in HSPC expansion medium with or without 30μM Nec1s or 5μM GSK8612 (TBK1 inhibitor) treatment. Cells were collected after 24 hours of culturing and p-NFκB and NFκB protein levels were compared by Western blotting.

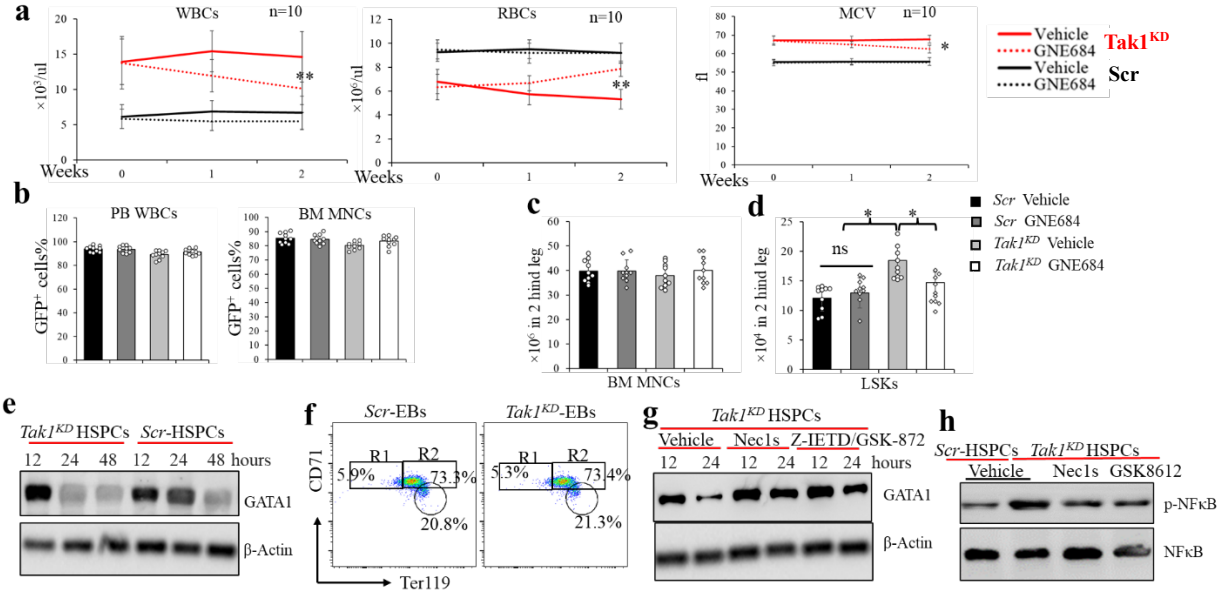

Figure S7. ***Tak1 inhibitor or cIAP inhibitor treatment selectively kills*** **Tak1^{KD}** ***HSPCs in vivo*** **(associated with Figure 5d-e)**. *sh2Tak1*-GFP-transduced HSPCs (*Tak^{KD}*) were mixed with non-transduced HSPCs (GFP$^-$) in a 1.5:1 ratio, whereas *scr*-GFP-transduced HSPCs were mixed with non-transduced HSPCs (GFP$^-$) in a 1:1 ratio. The mixed HSPCs were transplanted into lethally-irradiated mice. One-month post-transplantation, after determining the engraftment of the transduced HSPCs (GFP$^+$ cells in PB), mice were divided into three groups and treated with vehicle, HS-276 or birinapant, respectively, for two weeks. The mice were terminated 2 months later for PB analysis using Hemavet (**a**), and for examining GFP$^+$ cells within BM Lin$^-$c-Kit$^+$ HSPCs by flow cytometric analysis (**b**).

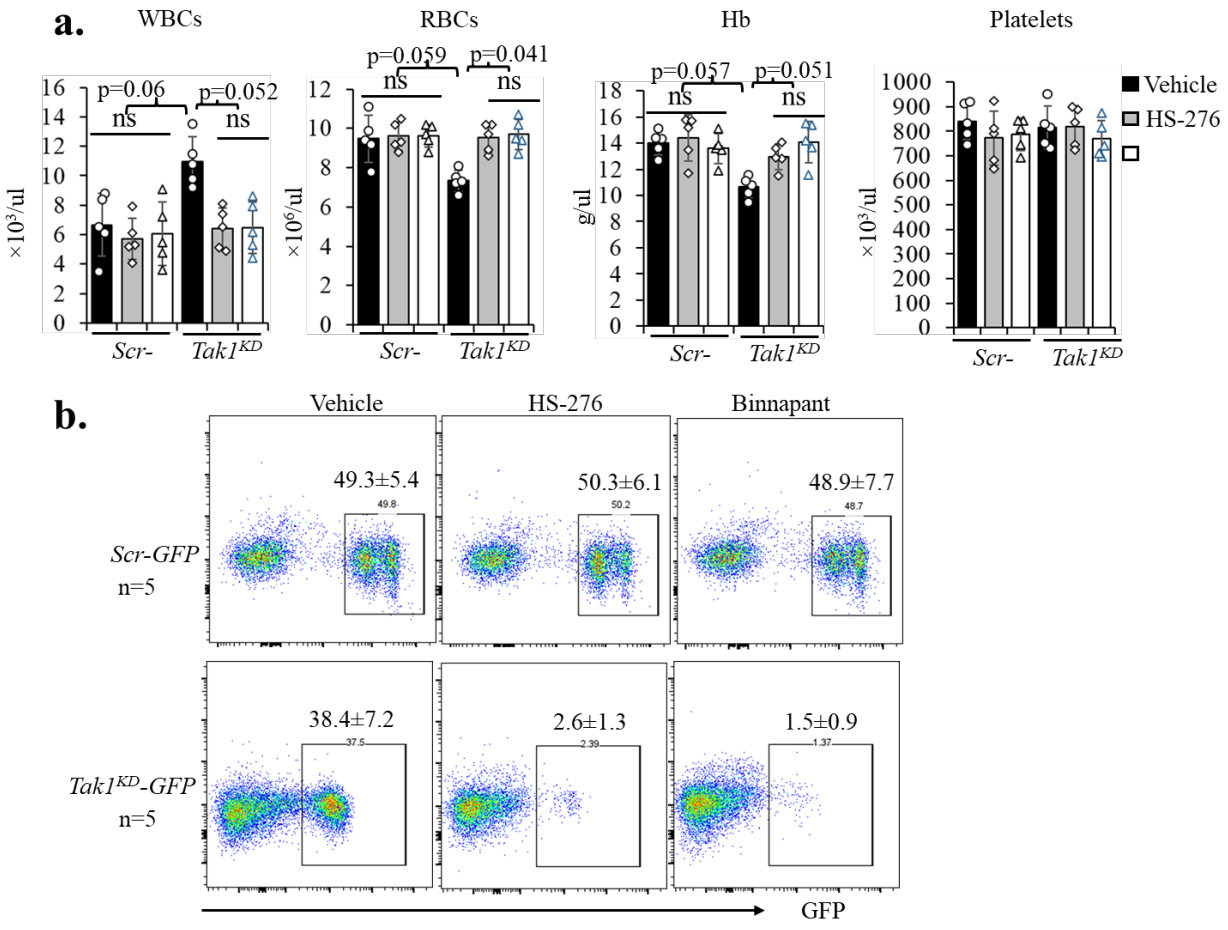

Figure S8. ***Inhibition of RIPK1 in human SF3B1^{mut} MDS samples*** **(associated with Figure 6b-g).** CD34^{+} HSPCs from HDs or MDS patients were cultured in 3-phase erythroid culture system with or without 100nM GSK3145095 treatment. Cells were collected on days 7 and 14 of culturing; BFU-E, CFU-E, Pro-EBs and early Baso-EBs were analyzed by flow cytometry on day 7 (**a**); late Baso-EBs, poly-EBs and ortho-EBs (**a**) and reticulocytes (**b**) were analyzed by flow cytometry on day 14. Representative flow cytometric data for analysis of erythroid precursors and EBs on indicated days of culture.[13]

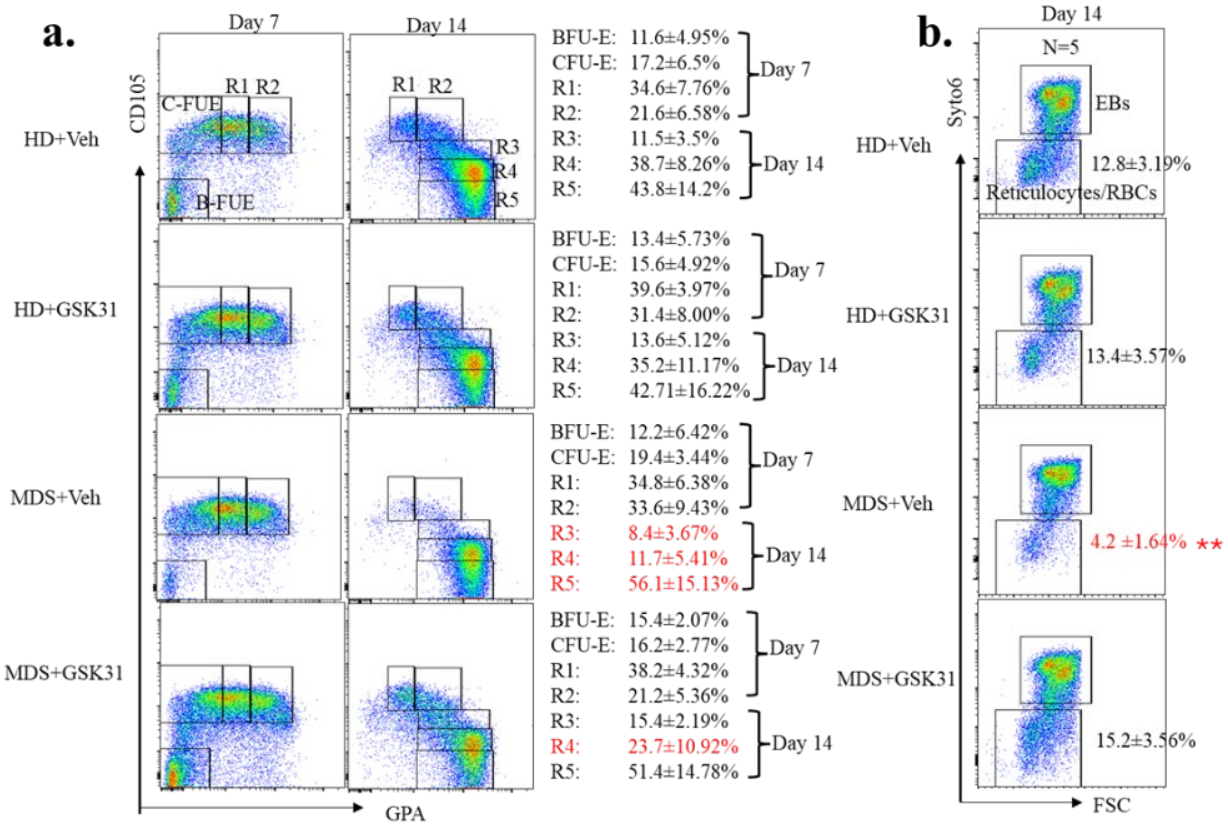

Figure S9. ***Inhibition of TAK1 in human SF3B1^{mut} MDS samples*** **(associated with Figure 6h-k).** CD34^{+} HSPCs from HDs or MDS patients were cultured in HSPC culture system. On day 2 of culturing, cells were treated with TAK1 inhibitor HS-276 or vehicle, respectively. **a.** Cells were collected on day 3 of culturing for intracellular anti-RIPK1 and anti-p-RIPK1 antibody staining followed by flow cytometric analysis for RIPK1 and p-RIPK1 protein levels. Representative flow cytometric data for analysis of RIPK1 and p-RIPK1 protein levels and cell death in HSPCs after HS-276 treatment. **b-c.** Cells were collected on day 4 of treatment for cell death analysis by Annexin-V and propidium iodide staining (**b**) and live cell counts (**c**). Isotype antibody staining was studied in parallel as a control in **a**.

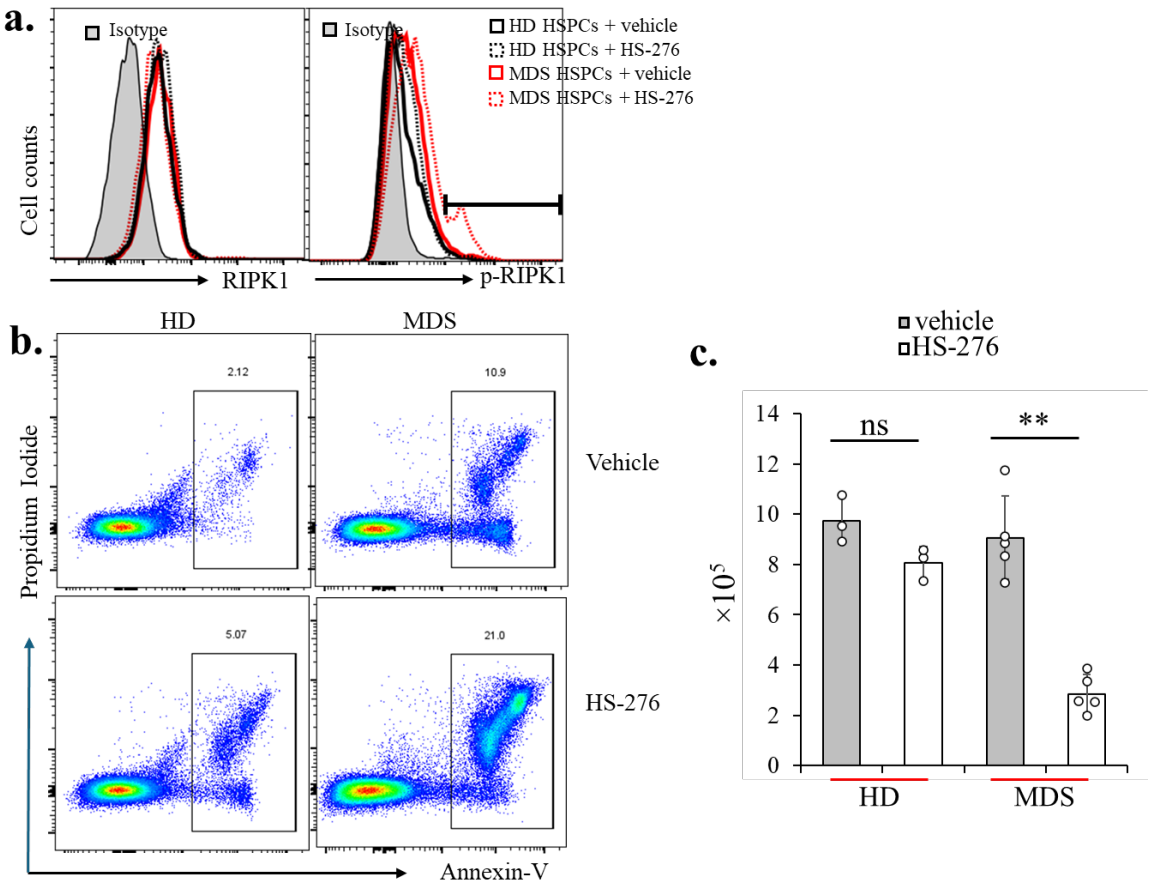

Original Western blotting data.

Figure 1e.

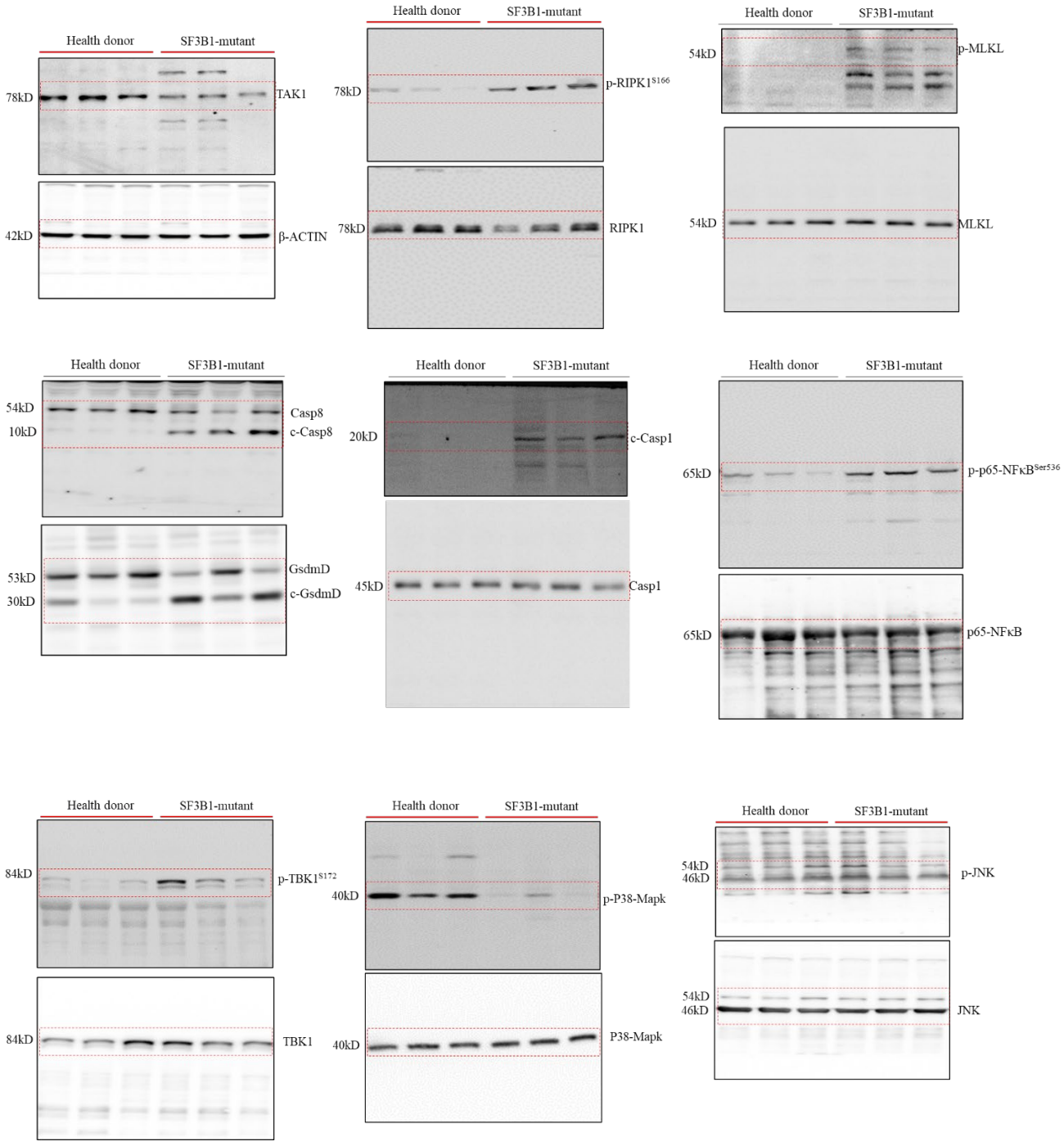

Figure 2d, f, and g.

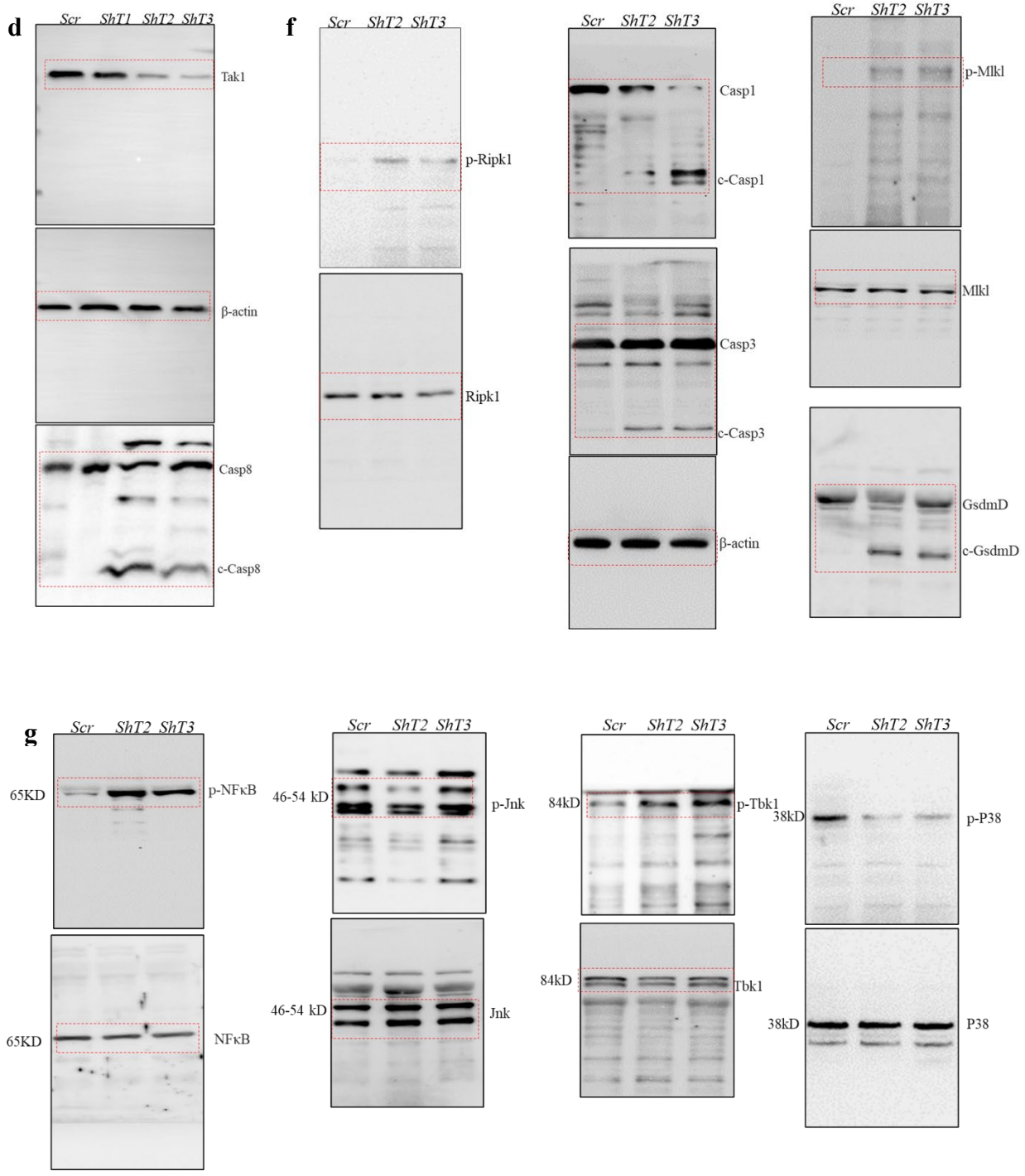

Figure S6e, g, and h.

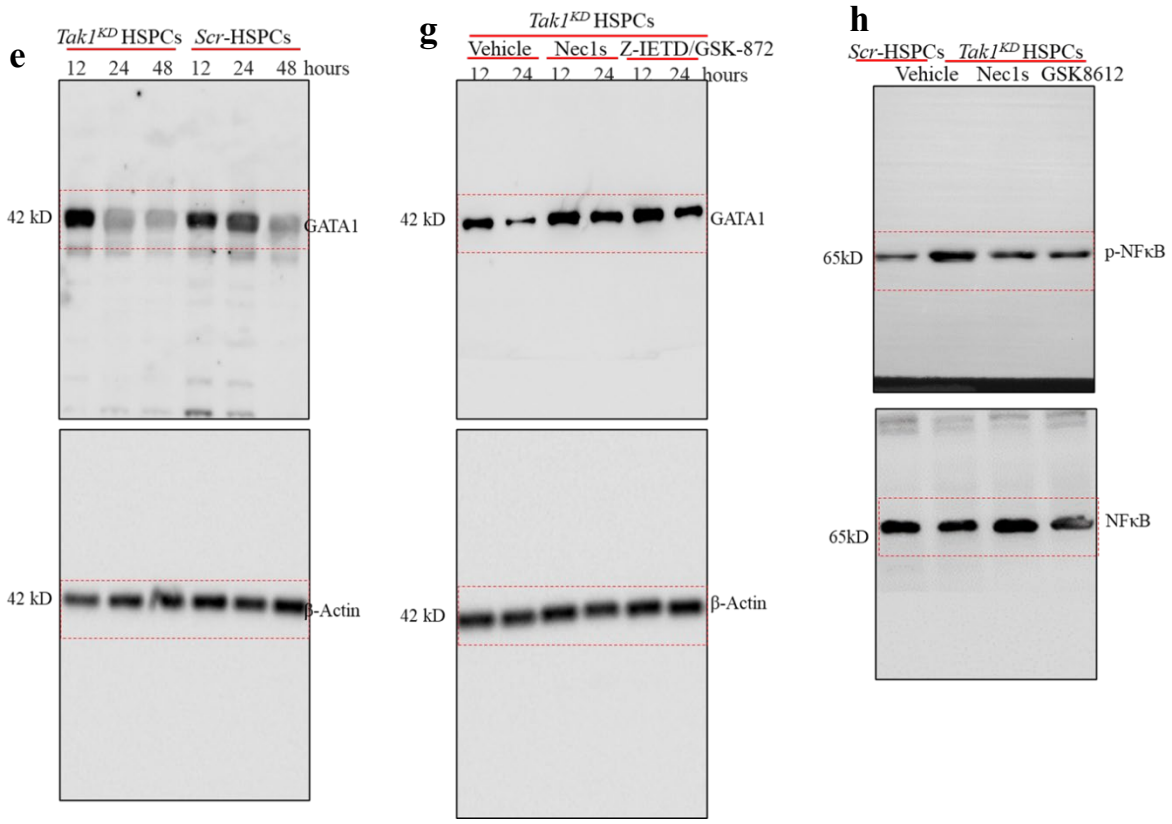

References

1. Wittmann N, Behrendt AK, Mishra N, et al. Instructions for Flow Cytometric Detection of ASC Specks as a Readout of Inflammasome Activation in Human Blood. *Cells.* 2021;10(11):2880.
2. Sester DP, Thygesen SJ, Sagulenko V, et al. A novel flow cytometric method to assess inflammasome formation. *J Immunol.* 2015;194(1):455-462.
3. Igarashi KJ, Kucinski I, Chan YY, et al. Physioxia improves the selectivity of hematopoietic stem cell expansion cultures. *Blood Adv.* 2023;7(14):3366-3377.
4. Tang M, Wei X, Guo Y, et al. TAK1 is required for the survival of hematopoietic cells and hepatocytes in mice. *J Exp Med.* 2008;205(7):1611-1619.
5. Liu S, Joshi K, Zhang L, et al. Caspase 8 deletion causes infection/inflammation-induced bone marrow failure and MDS-like disease in mice. *Cell Death Dis.* 2024;15(4):278.
6. Zhang L, Luo H, Ni HM, et al. Ripk3 signaling regulates HSCs during stress and represses radiation-induced leukemia in mice. *Stem Cell Reports.* 2022;17(6):1428-1441.
7. Aoto M, Iwashita A, Mita K, et al. Transferrin receptor 1 is required for enucleation of mouse erythroblasts during terminal differentiation. *FEBS Open Bio.* 2019;9(2):291-303.
8. Liu J, Zhang J, Ginzburg Y, et al. Quantitative analysis of murine terminal erythroid differentiation in vivo: novel method to study normal and disordered erythropoiesis. *Blood.* 2013;121(8):e43-49.
9. Chen K, Liu J, Heck S, et al. Resolving the distinct stages in erythroid differentiation based on dynamic changes in membrane protein expression during erythropoiesis. *Proc Natl Acad Sci U S A.* 2009;106(41):17413-17418.
10. Hu J, Liu J, Xue F, et al. Isolation and functional characterization of human erythroblasts at distinct stages: implications for understanding of normal and disordered erythropoiesis in vivo. *Blood.* 2013;121(16):3246-3253.
11. Sakurai M, Ishitsuka K, Ito R, et al. Chemically defined cytokine-free expansion of human haematopoietic stem cells. *Nature.* 2023;615(7950):127-133.
12. Challen GA, Pietras EM, Wallscheid NC, et al. Simplified murine multipotent progenitor isolation scheme: Establishing a consensus approach for multipotent progenitor identification. *Exp Hematol.* 2021;104:55-63.
13. Yan H, Ali A, Blanc L, et al. Comprehensive phenotyping of erythropoiesis in human bone marrow: Evaluation of normal and ineffective erythropoiesis. *Am J Hematol.* 2021;96(9):1064-1076.